

RAMAN EVIDENCE FOR THE
STRUCTURE OF THE
HYPONITRITE ION

by

JOHN EDWARD RAUCH

A THESIS

submitted to


OREGON STATE UNIVERSITY

in partial fulfillment of
the requirements for the
degree of

DOCTOR OF PHILOSOPHY

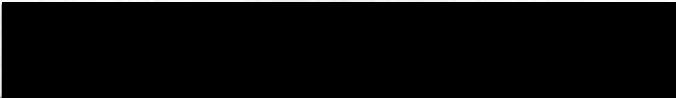
June 1962

APPROVED:




Professor of Chemistry

In Charge of Major



Chairman of Department of Chemistry



Chairman of School Graduate Committee



Dean of Graduate School

Date thesis is presented May 4, 1962

Typed by Mrs. J. E. Rauch

PARCHMENT DEED

ACKNOWLEDGEMENT

I dedicate this thesis to my wife Mary for her numerous valuable suggestions and her patience and understanding during the preparation of this thesis.

PARCHMENT DEED

SOUTHWORTH CO. U.S.A.

100% COTTON FIBER

TABLE OF CONTENTS

I	INTRODUCTION	1
II	DESIGN OF EQUIPMENT	3
III	SAMPLE PREPARATION	16
IV	OBSERVED SPECTRA	19
V	POLARIZATION OF RAMAN LINES	33
	A. THEORY OF THE POLARIZATION OF RAMAN LINES	33
	B. EXPERIMENTAL MEASUREMENT OF THE DEGREE OF DEPOLARIZATION OF THE 1383 cm^{-1} LINE OF $\text{Na}_2\text{N}_2\text{O}_2$	39
VI	THE GF MATRIX CALCULATION OF THE FORCE CONSTANTS OF THE HYPONITRITE ION	55
VII	A COMPARISON OF THE FORCE CONSTANTS CALCULATED FOR THE HYPONITRITE ION WITH THE FORCE CONSTANTS OF SIMILAR SYSTEMS	83
VIII	CONCLUSION	86
	BIBLIOGRAPHY	87

PARCHMENT DEED

SOUTHWORTH CO. U.S.A.

100% COTTON FIBER

LIST OF ILLUSTRATIONS

Stainless Steel Electrode for Lamp	8
Low Pressure H _g Lamp	9
Photographs of Lamp Assembly	10
Diagram of Optical System	11
Hilger E612 Spectrograph	12
Visible Absorption Curve for Sat. Aq. NaNO ₂	13
Visible Absorption Curve for Rhodamine Treated Cellophane	14
Sample Tube	15
Negative Logarithm of k Versus Temperature	21
β Versus Temperature	22
Log (Rate of N ₂ O Evolution) Versus pOH	23
Concentration of Sodium Carbonate Versus Equivalent Time	24
Internal Standardization for CO ₃ ⁼ Impurity Determination	25
Raman Spectrum	30
Infrared Spectrum	31
Photographic Reproduction of the Plate Showing the Raman Spectrum of Aq. Na ₂ N ₂ O ₂	32
Visible Absorption Curve for HN32 Linear Polaroid	42
The Observed Value of ρ Versus the Values of ρ Obtained by Crawford and Horwitz	46
Internal Calibration for CCl ₄ Plate	48
Internal Calibration for C ₆ H ₆ Plate	50
Internal Calibration for CHCl ₃ Plate	52
Internal Calibration for Aq. Na ₂ N ₂ O ₂	54

LIST OF ILLUSTRATIONS continued

$F_{r\alpha}$ Versus F_r	72
$F_{r\alpha}$ Versus F_α at Various Values of r_2/r_1	73
F_{Rr} Versus r_2/r_1 at 120° and $F_{r\alpha} = 0$	77
α Versus $F_{R\alpha}$ at $r_2/r_1 = 1.135$	78
α Versus F_R at $r_2/r_1 = 1.135$	79
α Versus F_{Rr} at $r_2/r_1 = 1.135$	80

PARCHMENT DEED

SOUTHWORTH CO. U.S.A.

100% COTTON FIBER

RAMAN EVIDENCE FOR THE STRUCTURE OF THE HYPONITRITE ION

CHAPTER I INTRODUCTION

The structure of the hyponitrite ion has been discussed in several papers, but a complete description of the ion has been lacking. This has resulted partly because in all the structures conceived for this ion, the number of observed Raman and infrared fundamental vibrational frequencies did not coincide with the number of predicted frequencies. Kuhn and Lippincott (9, p. 1820-1821) assigned to the ion C_{2h} symmetry based on the number of observed frequencies and their mutual exclusion in the Raman and infrared spectra. Later, Millen et al. (12, p. 18) observed a slightly different set of values for the infrared and Raman frequencies but with essentially the same result. They (13, p. 687-691) also made some approximate force constant calculations to show that C_{2h} symmetry was allowable from the observed spectra. In their discussion they predicted two new low frequencies, one in the Raman belonging to the A_g species and one in the infrared belonging to the B_u species, which would be consistent with C_{2h} symmetry.

The work presented in this thesis was undertaken with the view that more Raman information was obtainable from

the hyponitrite ion. Since the two already observed Raman lines and the third, as yet unobserved, line necessarily belonged to the A_g species if the ion was to have C_{2h} symmetry, these lines should have depolarization ratios between 0 and $6/7$. Thus, if the depolarization ratio could be measured as positively less than $6/7$, then the lines must belong to the A_g species since the lines associated with all other species have depolarization ratios of $6/7$. Also if there was a third Raman fundamental, it was thought that improved technique in preparing the sample and handling the sample during exposure could result in seeing this third line. Three Raman lines assignable to the hyponitrite ion were observed in this study. Two lines were identical with those observed by Millen et al. Thus, one will find in this paper a discussion of the force constants which would arise from these three Raman lines.

PARCHMENT DEED

SOUTHWORTH CO. U.S.A.

CHAPTER II

DESIGN OF EQUIPMENT

The equipment used to carry out this study was designed to use the H_g 4358 \AA line to excite the molecule. Thus, methods were needed to excite the mercury spectrum, isolate the 4358 \AA line, pass this near monochromatic light through the sample, and observe the resulting change in the exciting light.

H_g LAMP

The lamp was a modification of a low pressure H_g lamp described by Haunschild (7, p. 4-11) in which tap water was run through stainless steel electrodes (page 8) to cool the lamp. See page 9 for a drawing of the lamp.

This lamp was longer (the lamp in the illuminating region was of a smaller diameter) and four stainless steel fittings were employed instead of three in comparison to Haunschild's lamp. The lamp was usually operated at 10 amperes of current. At this current there was a voltage drop of 36 volts across the lamp. A ballast resistor of about 3.4 ohms was included in the circuit.

In starting the lamp a vacuum of about 4 microns of mercury pressure was first attained. Then the lamp would start with or without the tap water flowing through the electrodes and with or without the lamp connected to

the vacuum line (the lamp was usually continuously connected to the vacuum system during operation). The lamp was found to start readily if across the upper cold finger electrodes the voltage from a luminous gas tube transformer was impressed and simultaneously the mercury pool was activated through the glass wall at the surface of the mercury pool with a spark tester. The voltage across the mercury electrodes was kept at about 110 volts during this process. Upon starting the current would rise to about 28 amperes with this voltage across the system.

Actual photographs of the lamp may be seen on page 10. The upper picture shows the lamp in operation.

OPTICAL ARRANGEMENT

The optical arrangement which is diagramed on page 11 corresponds to the design suggested by Nielson (16, p. 494-499) for the efficient filling of a spectrograph with light from a Raman tube using a condensing lens. The focal length of the condensing lens was 65.6 mm. The effective diameter of the sample tube was 9.34 mm. (The actual diameter was 15.0 mm.) The prism height was 86 mm. The best slit height was 2.88 mm. The focal length of the collimating lens was 5.84 mm. The distance from the slit to the condensing lens, z , was 85.8 mm. The distance from the condensing lens to the front end of the Raman

tube, x , was 17 mm. The assumed index of refraction of the sample was 1.33 (water). The effective length of the Raman tube was 395 mm. For the data obtained in this thesis the slit width was 0.10 mm.

SPECTROGRAPH

The spectrograph used was the commercially available Hilger E612 Raman spectrograph with the F5.7 camera attachment (E614). For a diagram of the spectrograph see page 12.

FILTER SYSTEM

The filters used to isolate the $4358 \text{ \AA} \text{ H}_g$ line from the lamp were illustrated by Stamm (20, p. 318-331). A one centimeter path of saturated aqueous NaNO_2 was used to reduce the light of higher frequency than 4358 \AA . See the diagram on page 13 for an absorption curve of this solution. This filter was circulated through the filter jacket which is shown in place in the lower left picture on page 10, and cooled by passing water through a coiled glass tube immersed in a reservoir of the filter solution. Instead of using the 0.5 cm. path of Rhodamine 5GDN Extra, 0.075 gram per liter (aq.), an equivalent filter was designed which had a similar absorption in the visible region with the advantage of

requiring less space. This was made by placing a sheet of uncoated cellophane, DuPont cellophane 600PD, in an aqueous solution of Rhodamine 5GDN Extra, 0.075 gram per liter, for about one hour. The absorption curve in the visible region for the filter used in this series of experiments prepared in the manner mentioned above is illustrated in the diagram on page 14. This filter was wrapped tightly around either the sample tube or a polaroid cylinder, whichever was appropriate to the experiment at hand.

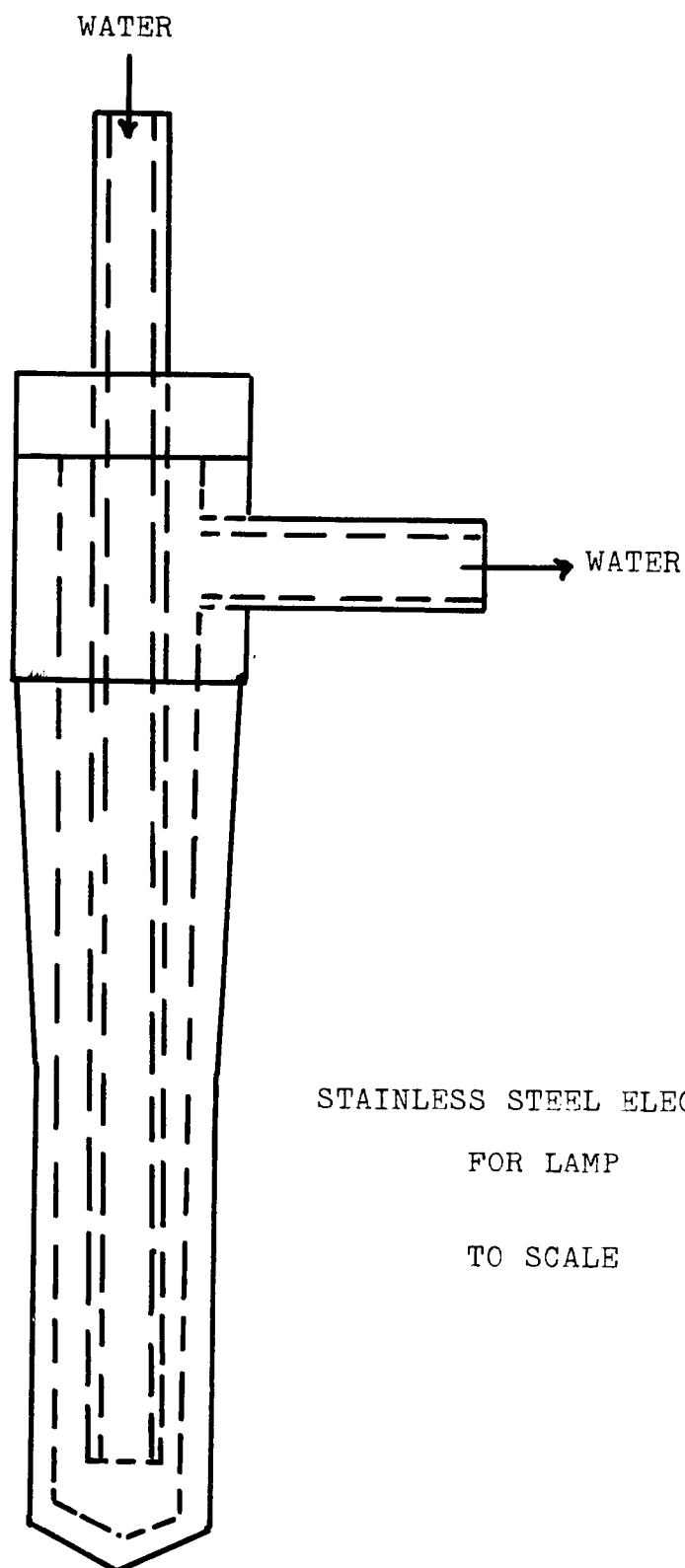
SAMPLE TUBE AND SAMPLE TUBE HOLDER

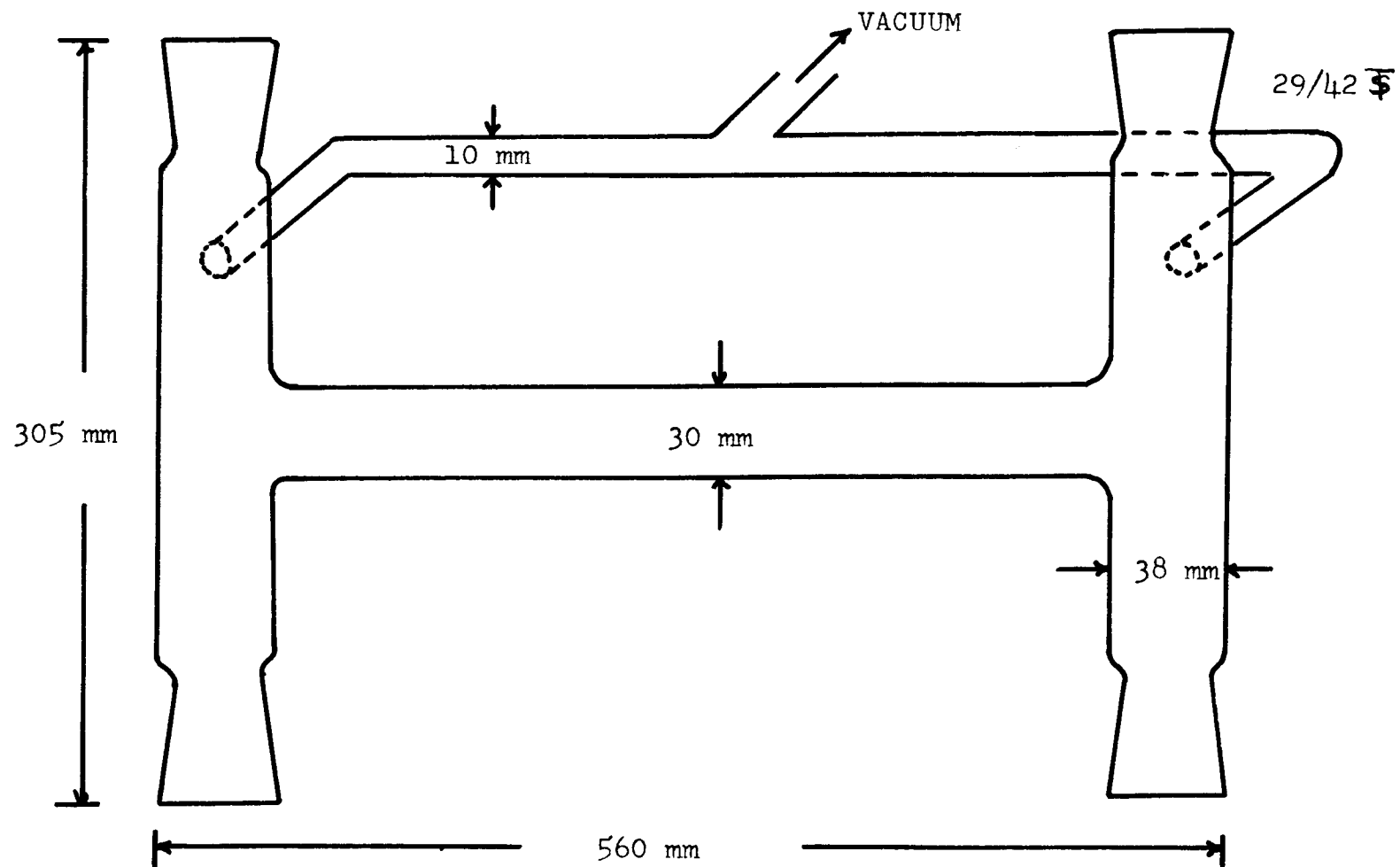
The sample tube was essentially a Wood's type tube made of constant bore tubing of 15.0 mm. diameter. See diagram on page 15. The back portion of the tube was bent so that the opening could be kept upright when the tube was in place. The portion of the tube which was not illuminated and the cap were painted with a heavy coat of black enamel. The sample tube holder and its relation to the sample tube are illustrated by the photographs on page 10. The tube holder was supported on an extension of the spectrograph on a triangular mounting to insure proper alignment. The correct position of the tube was assured by a cone shaped rest for the front of the tube and a V shaped support for the rear of the tube.

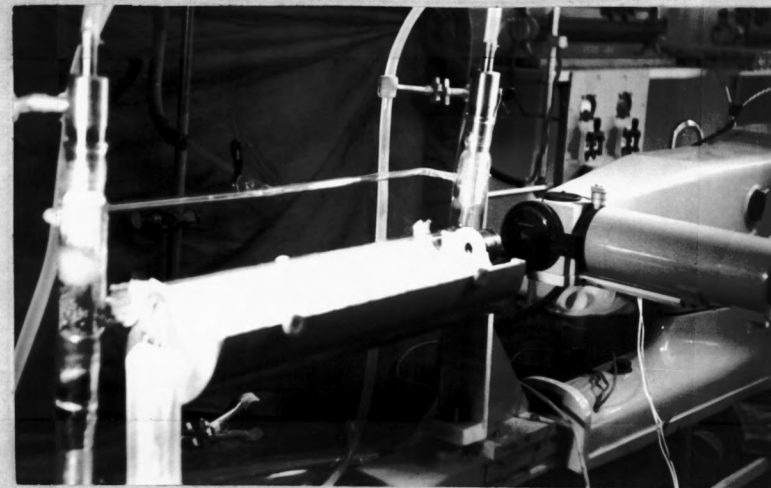
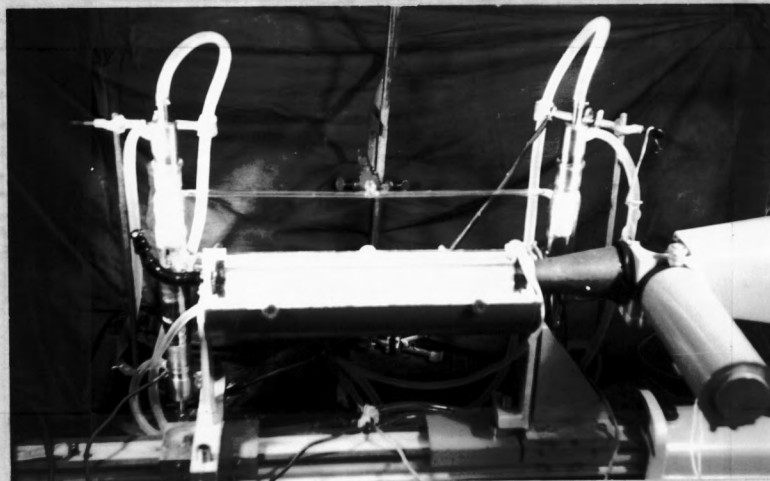
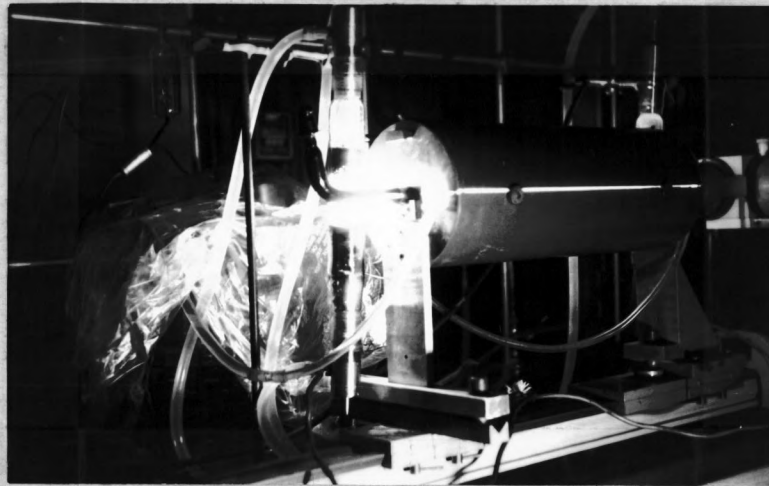
PHOTOGRAPHIC PLATES AND PROCESSING

Kodak 103a-0 spectroscopic plates were used throughout the experiment. These plates show good sensitivity in the $4358 \text{ \AA}^{\circ} \text{ H}_g$ line region but become insensitive after about a 3000 cm^{-1} shift on the red side of this line. The plates were developed for two minutes at about 25°C (room temperature) with D-8 diluted one part D-8 to two parts water (4, p. 268-274). After development they were placed in an acetic acid stop bath for about 30 seconds and then fixed for about 10 minutes in Kodafix diluted one part Kodafix to three parts water. After washing the plates were placed in Farmer's reducer solution A (3.75 g. $\text{K}_3\text{Fe}(\text{CN})_6$ per liter) for two minutes and then in solution B for five minutes. After the hypo had been washed out the plate was placed in a Kodak Photo-Flo solution for about 30 seconds before drying.

The opacities of the lines of the plates were recorded with a Jarrell Ash #2105 Microphotometer. For the use of this instrument I am indebted to the Bureau of Mines in Albany, Oregon, and in particular Mr. George Kantas.







PHOTOGRAPHS OF LAMP ASSEMBLY

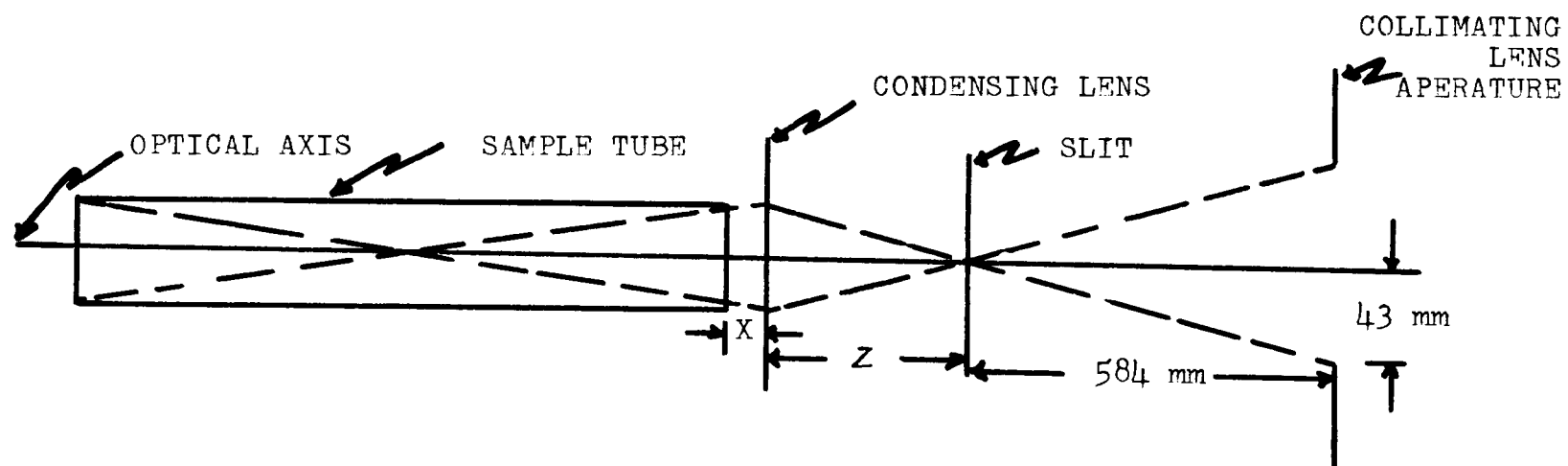
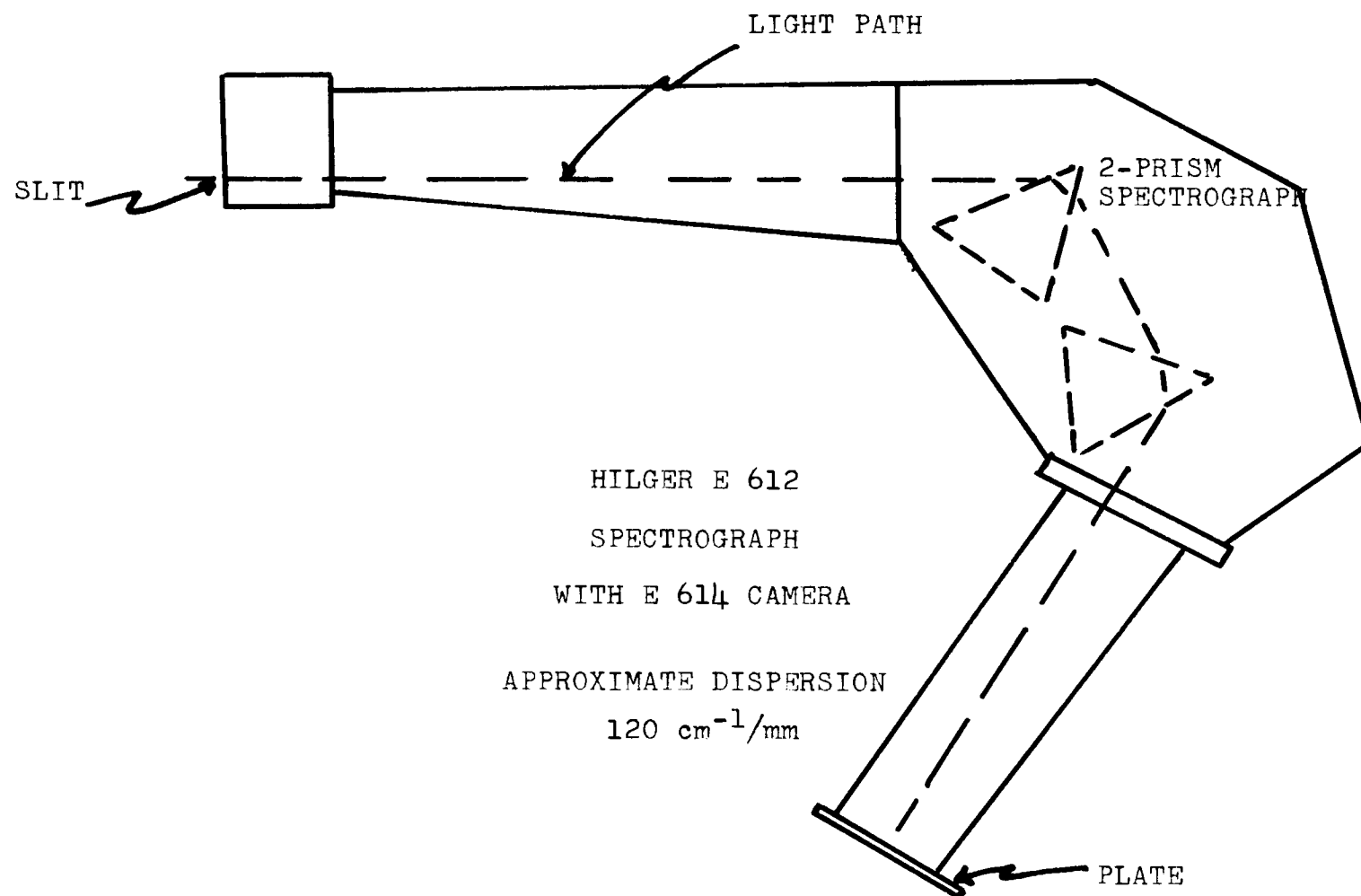
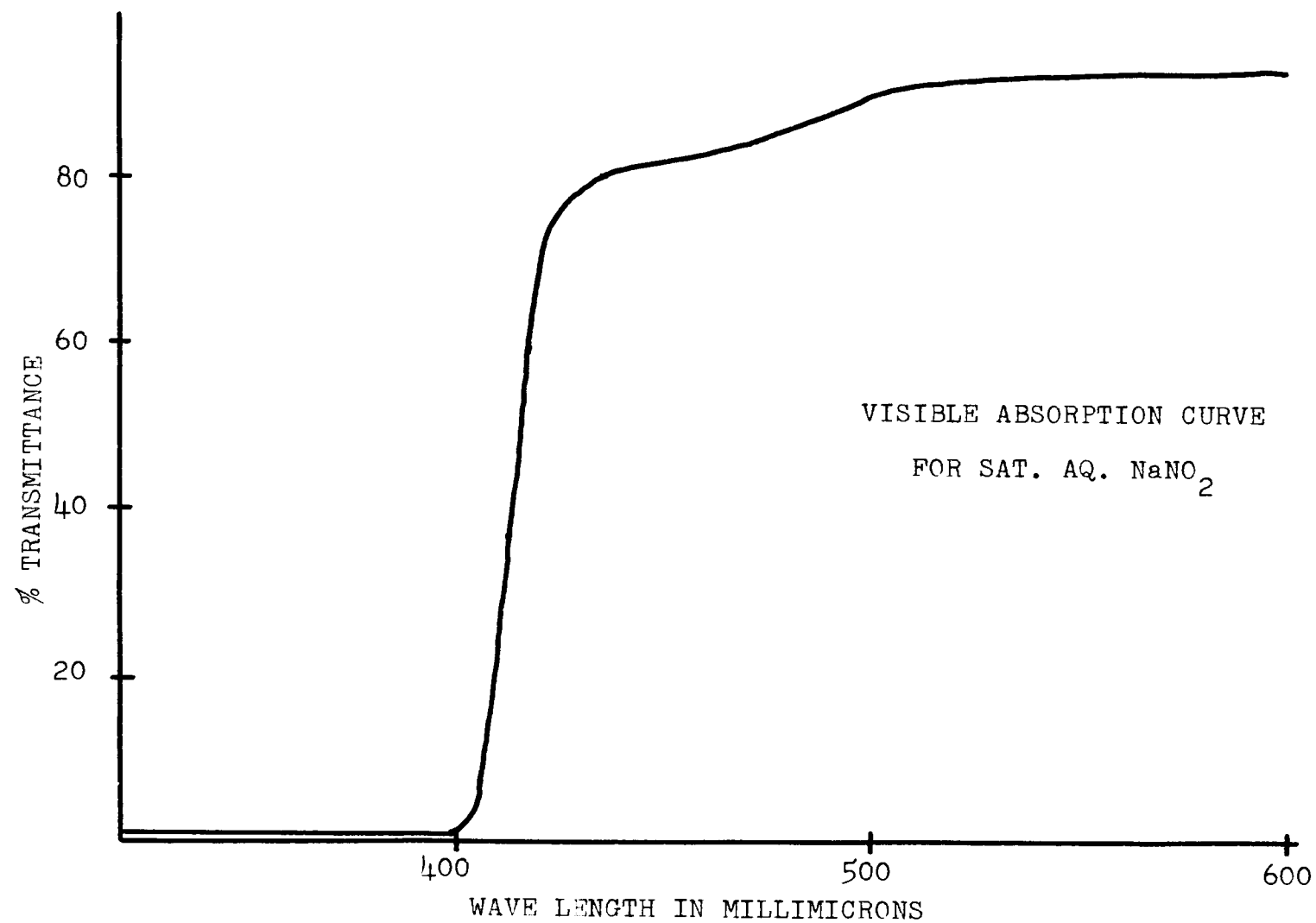
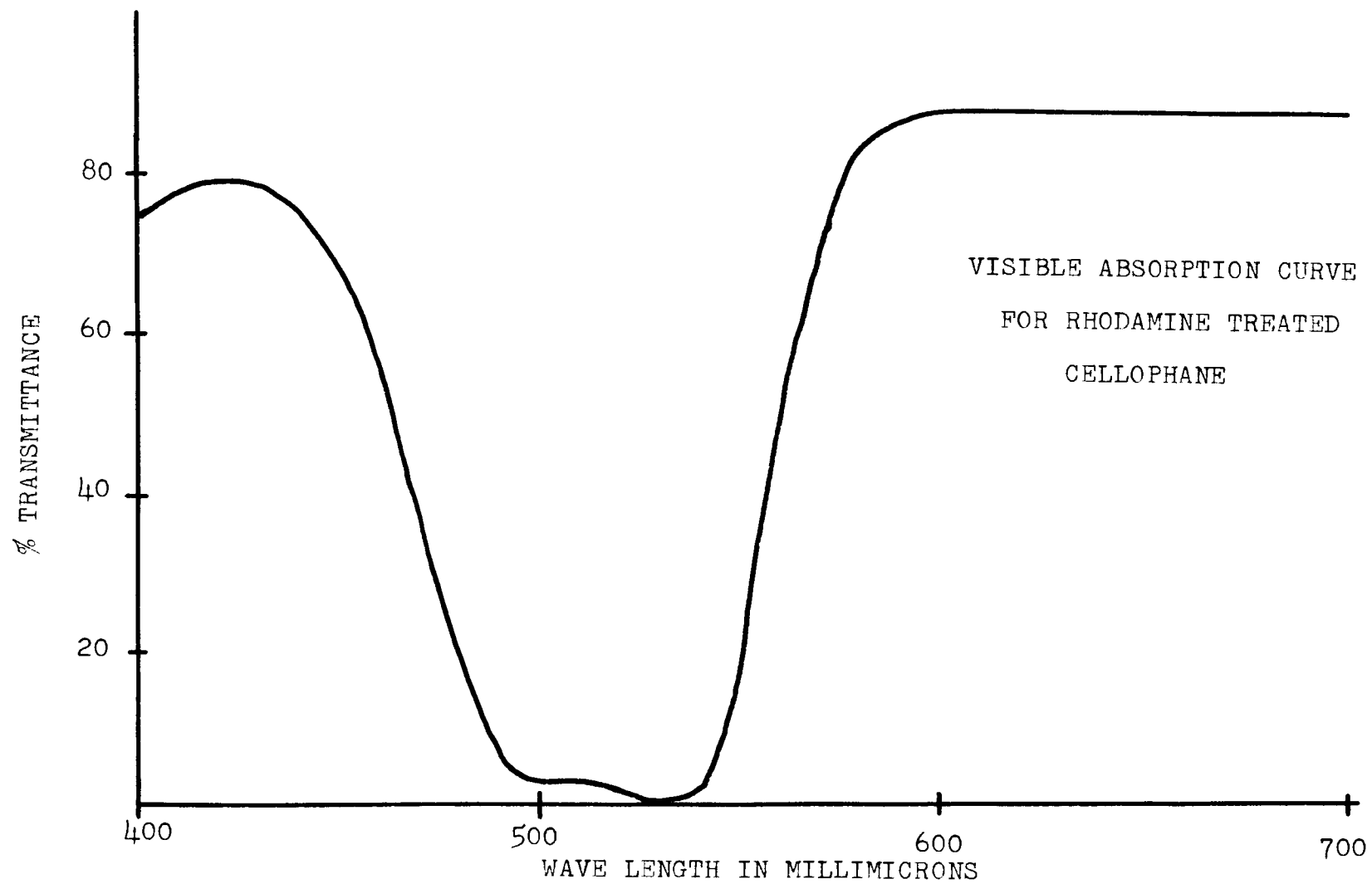
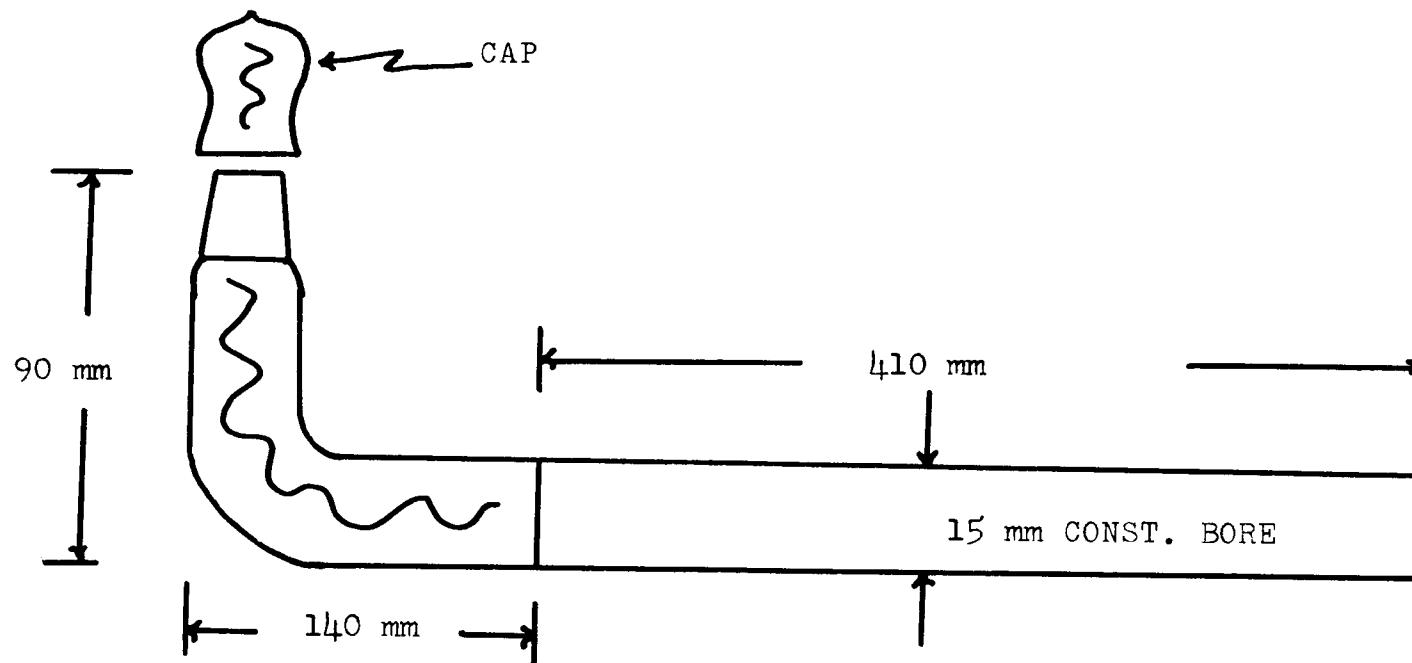


DIAGRAM OF OPTICAL SYSTEM





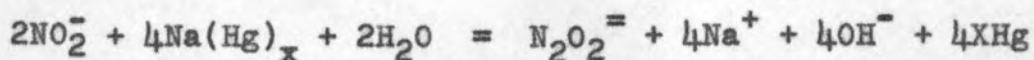




SAMPLE TUBE

CHAPTER III
SAMPLE PREPARATION

The sodium hyponitrite was prepared essentially by the method described by Partington and Shah (17, p. 2071-2080). In this method an aqueous solution of sodium nitrite is reduced to sodium hyponitrite with sodium amalgam.



One hundred grams of Mallinckrodt U.S.P. sodium nitrite were dissolved in 200 cc. of distilled water. The sodium amalgam was prepared by slowly adding 100 grams of Baker reagent sodium to 555 cc. of mercury. After the aqueous solution was poured into a 2-liter round bottom flask and placed so that tap water could continuously cool the flask, the amalgam was slowly added. After the reaction had cooled and had been cool for at least one hour, the unreacted amalgam was separated from the reaction mixture. The reaction mixture was not shaken at this point (17, p. 2071-2080) since this tended to cause difficulties in the following filtration. The thick mixture was then filtered through Scientific Supplies filter paper number 28320 into a Büchner funnel. A stream of carbon dioxide free air or nitrogen should have been blown over the mixture at this point since the mixture was extremely basic and absorbed carbon dioxide from the air. The lack of this precaution probably

caused the carbonate contamination of the sodium hyponitrite. The solid, impure sodium hyponitrite was repeatedly triturated with absolute ethanol until the solid would fall freely. The mixture was then filtered and washed with absolute ethanol.

At this point the collection of samples from two or three runs was used. The impure sodium hyponitrite was dissolved in the least amount of water. This solution was added to about 25 grams of activated charcoal and mixed. After about five minutes the mixture was filtered. The aqueous solution was concentrated by placing the sample in a capped jar (the lid was screwed on loosely) which held about twice the volume of liquid present and then putting this jar in a vacuum desiccator which had concentrated sulfuric acid as a desiccant. The desiccator was evacuated with a fore-pump using a dry ice-acetone cooled trap to prevent the water from contaminating the fore-pump oil. Caution should be used at this point not to dry the sample too fast or too much since the octahydrate form probably has superior properties to the anhydrous form for purification.

After the sample had crystalized it was repeatedly triturated with absolute ethanol, filtered, washed with ethanol, and finally washed with absolute ether. Then the sample was dried over concentrated sulfuric acid at about 20 microns of mercury pressure.

An infrared spectrum of the sample at this stage showed the presence of carbonate and nitrite of which the nitrite could be almost entirely removed by repeating the process of dissolving the sample in water and allowing the octahydrate to precipitate. A medium intense band at 885 cm^{-1} appeared which could not be assigned to either carbonate or nitrite, but it tended to be removed upon trituration of the sample with absolute ethanol. Whether this band was due to NaNH_2O_2 was not investigated further. This line was reported by Kuhn and Lippincott (9, p. 1820-1821) but they did not give it an assignment.

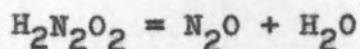
The yield was about 19 percent of the theoretical yield.

CHAPTER IV

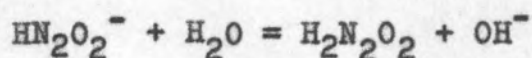
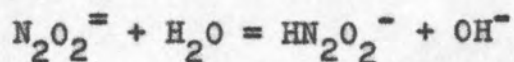
OBSERVED SPECTRA

Just prior to making the Raman exposures of the aqueous $\text{Na}_2\text{N}_2\text{O}_2$, 50.0 grams of $\text{Na}_2\text{N}_2\text{O}_2 \cdot x\text{H}_2\text{O}$ and 4.00 grams of reagent NaOH were dissolved in 140 cc. of solution. During the solution process the sample was cooled in an ice bath to avoid decomposition due to the heat generated upon solution. The solution was then filtered three times through a Corning fine sintered glass filter. During the filtering process the filter was capped with a tube containing ascarite so that the atmospheric air was required to pass through the ascarite tube.

NaOH was added to the solution to retard decomposition of the hyponitrite. If the rate determining step for the decomposition of the hyponitrite ion in water is (23, p. 55)



the derived kinetic equation explains reasonably well the experimental findings on the rate of decomposition of hyponitrite. Thus one may write



$$K_1 = \frac{[\text{HN}_2\text{O}_2^-] [\text{OH}^-]}{[\text{N}_2\text{O}_2^{=}]}$$

$$K_2 = \frac{[H_2N_2O_2][OH^-]}{[HN_2O_2^-]}$$

and

$$\frac{d[N_2O]}{dt} = k' [H_2N_2O_2]$$

Then if one lets

$$[N_2O_2^-]_s = [N_2O_2^-] + [HN_2O_2^-],$$

the final result is

$$\frac{d[N_2O]}{dt} = \frac{K_2 k' [N_2O_2^-]_s}{[OH^-] \left(1 + \frac{[OH^-]}{K_1}\right)}$$

Let

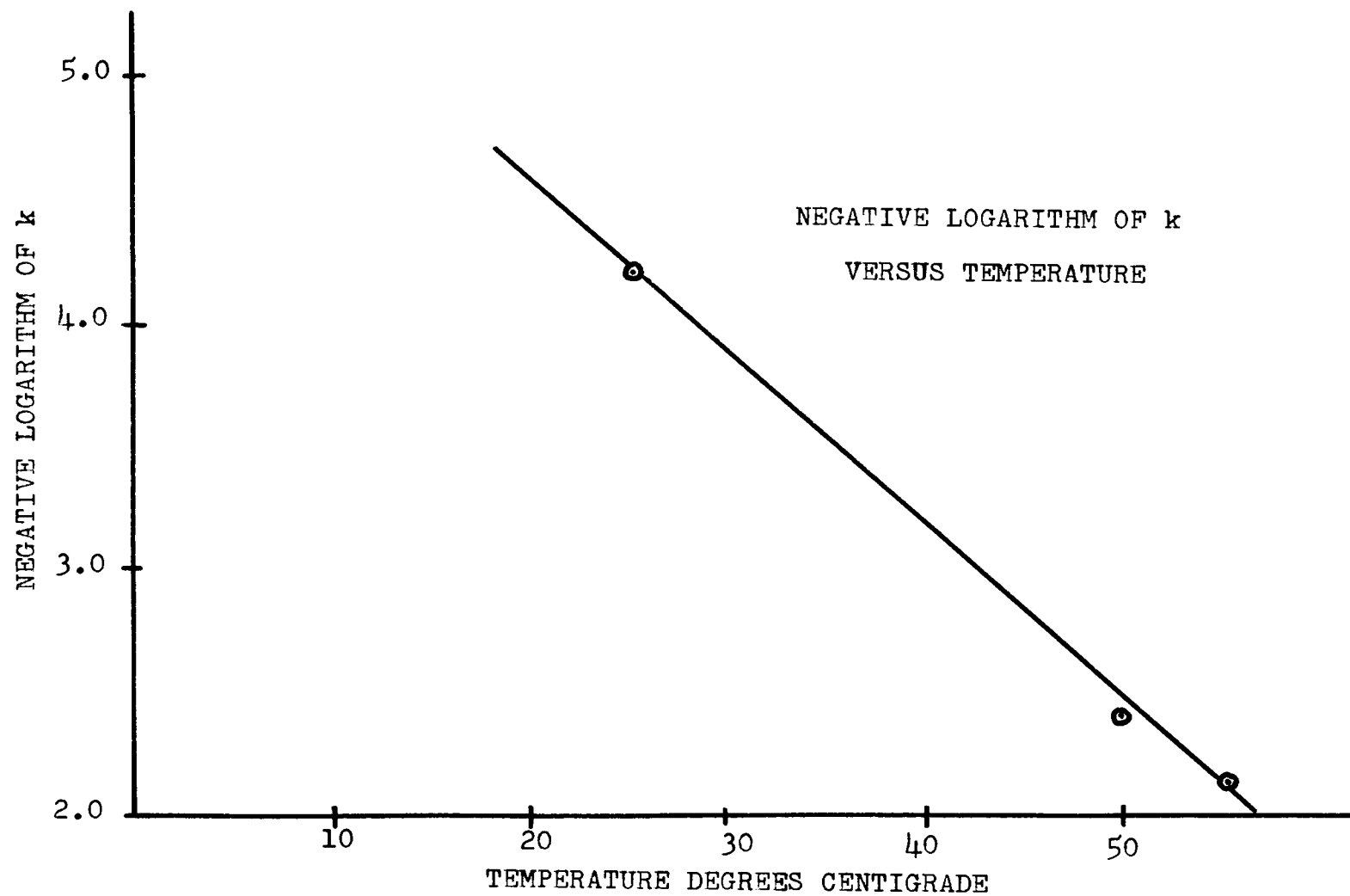
$$K_2 k' = k$$

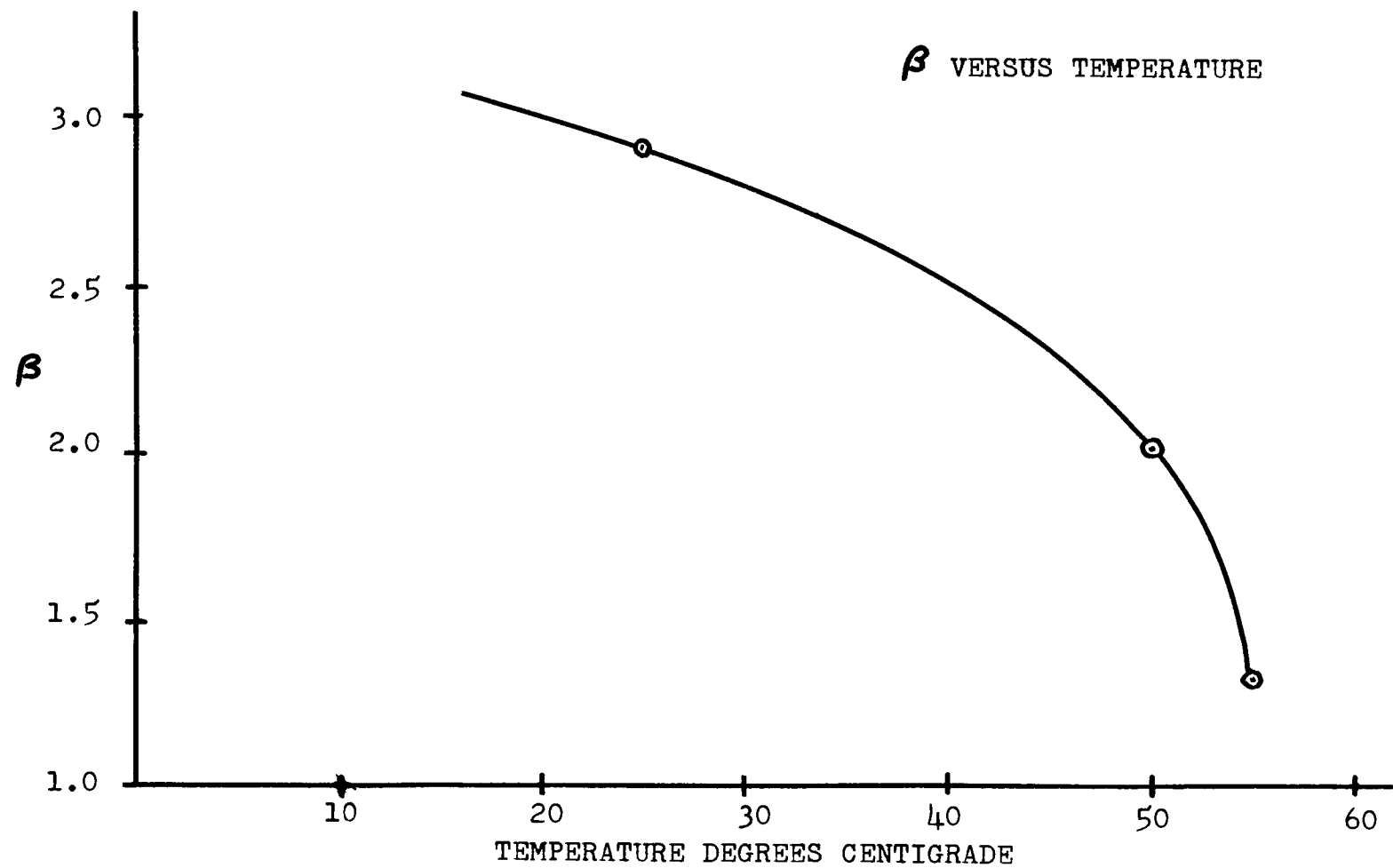
and

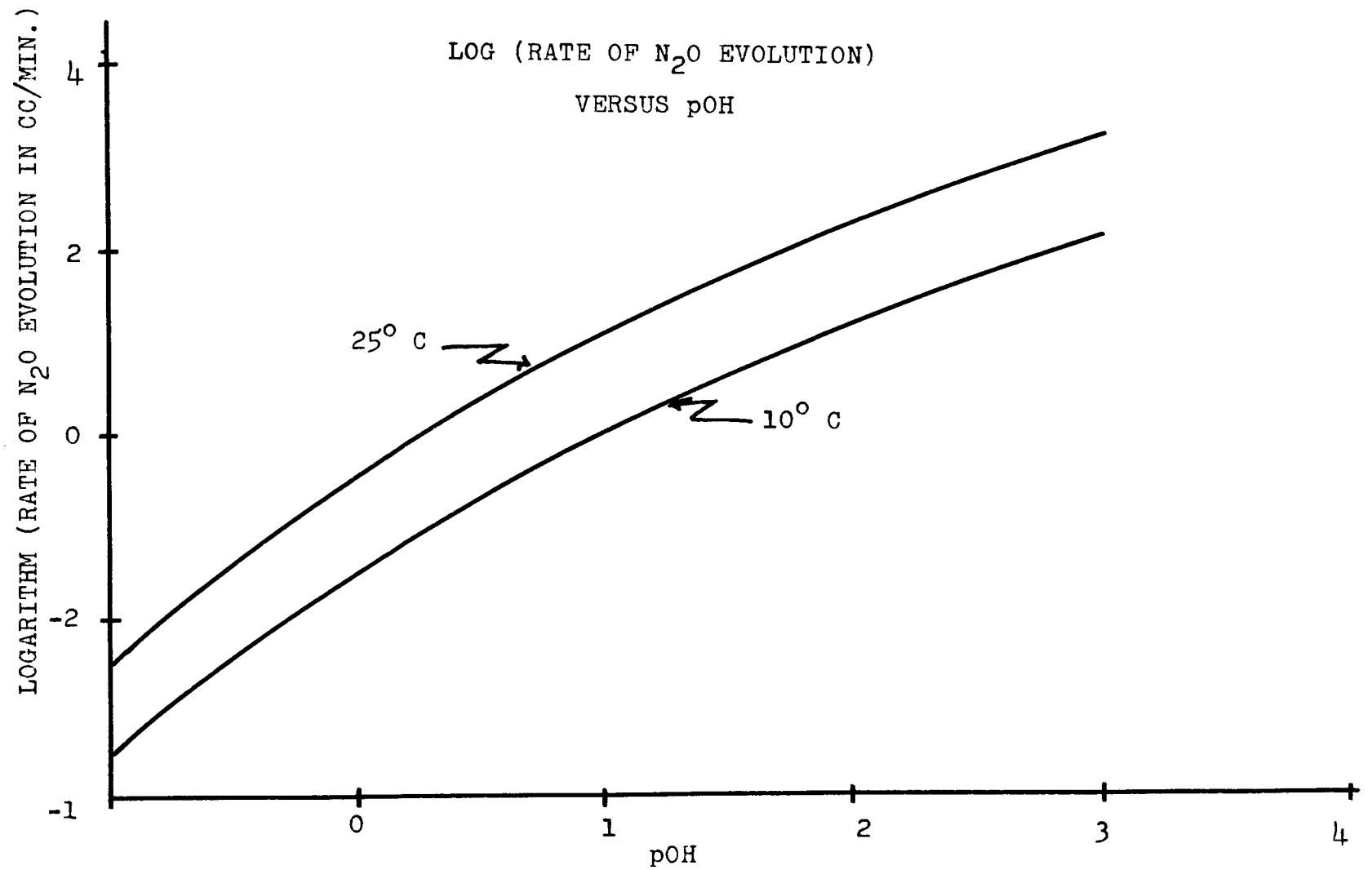
$$\frac{1}{K_1} = \beta$$

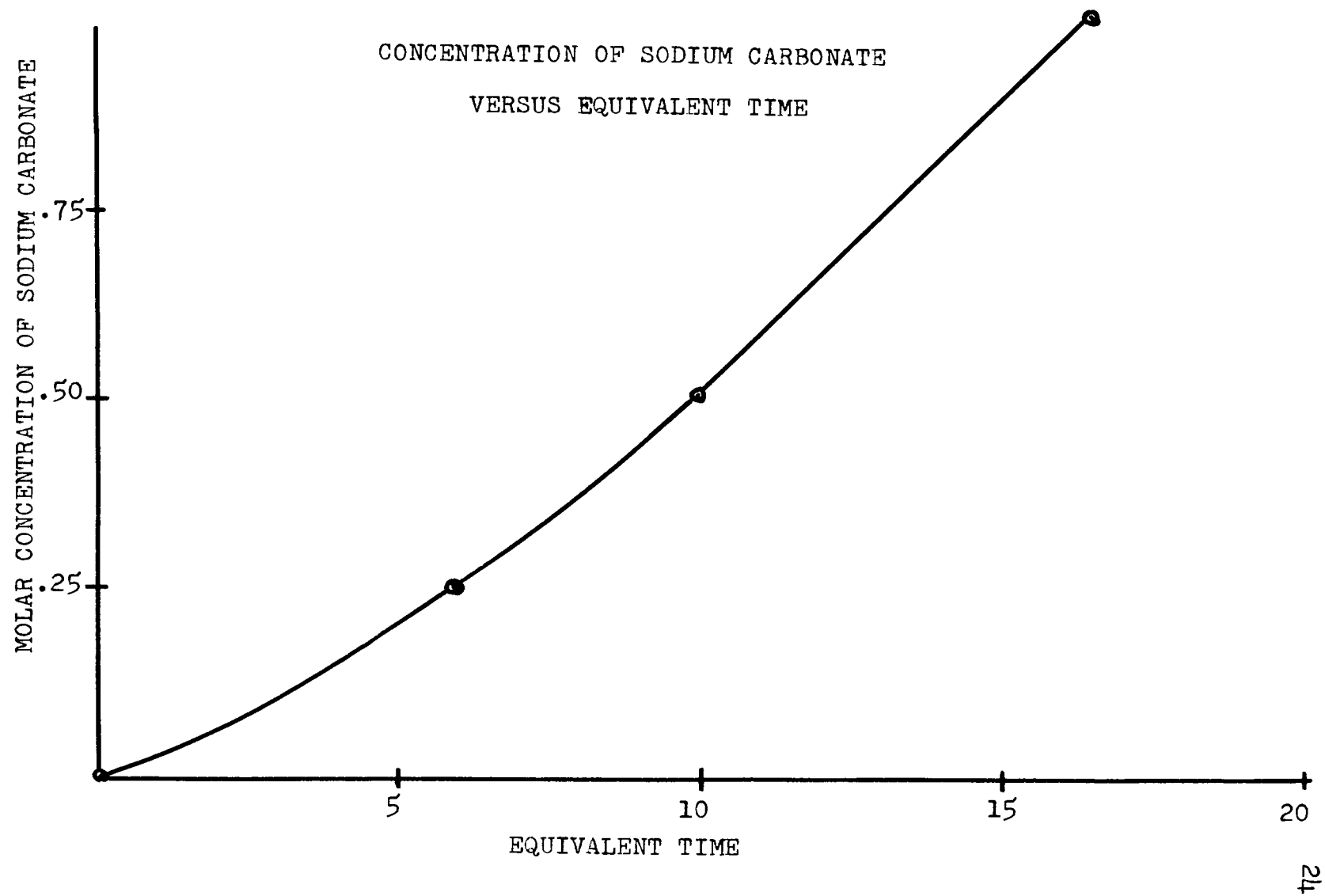
A plot of -logarithm k versus the temperature is shown on page 21. A plot of β versus the temperature is shown on page 22. On page 23 a plot of the logarithm of the rate of N_2O evolution versus the $[OH^-]$ is shown for $25^\circ C$ and for $10^\circ C$. Thus, it is easily shown that several orders of magnitude reduction in the rate of the decomposition of the hyponitrite ion may be attained if the solution is made 1 M NaOH as compared to the addition of no NaOH. Also a reduction in the rate of decomposition is obtained in cooling the sample.

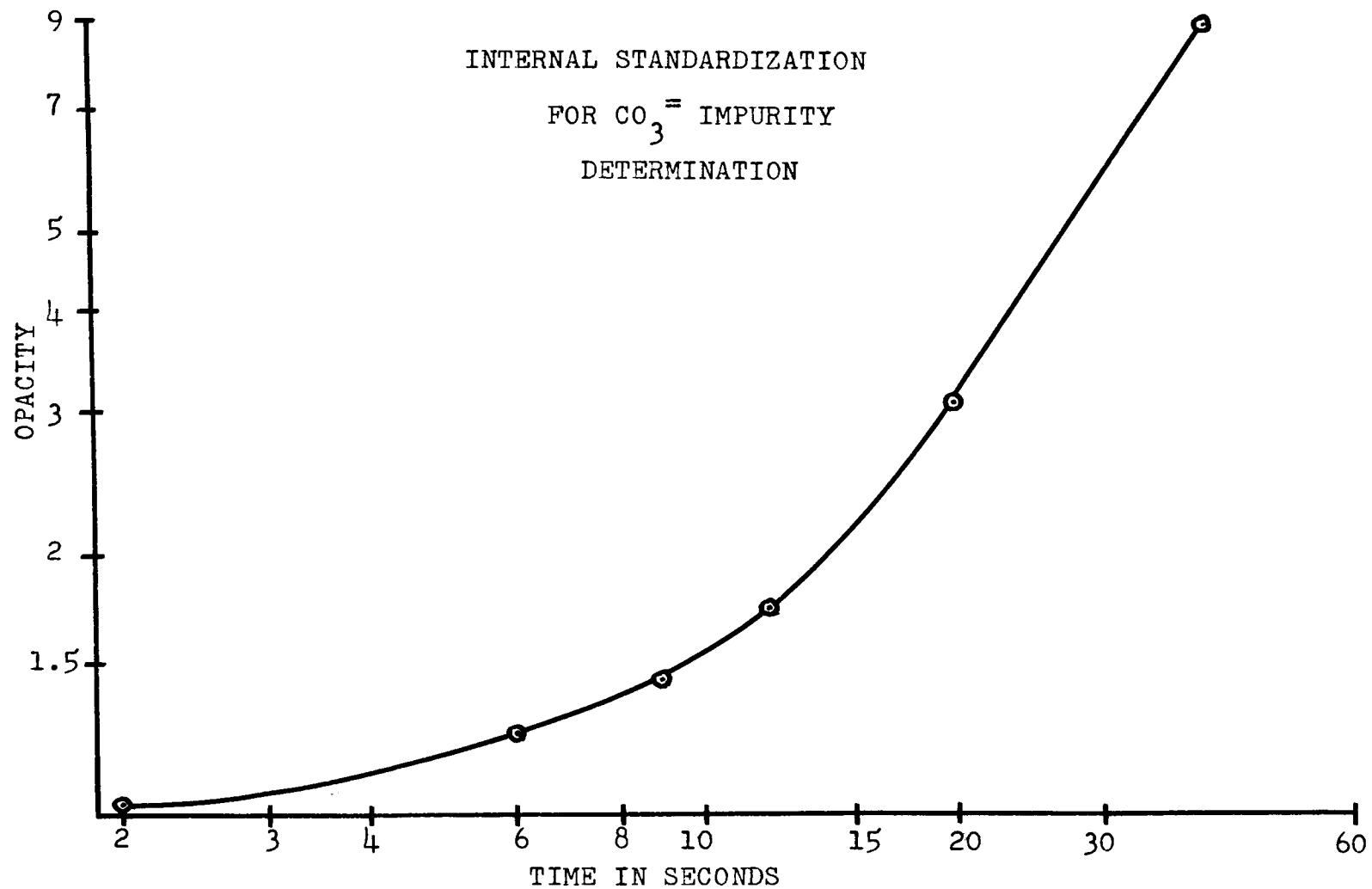
The sample was cooled to near the temperature of tap











water by circulating the NaNO_2 filter solution through the filter jacket. The filter solution was in turn cooled by passing tap water through a coiled glass tube immersed in the filter solution.

The exposure was made for one half hour with 15.0 amperes passing through the lamp. On the same plate samples of 1.00 M Na_2CO_3 in 1.00 M NaOH, 0.50 M Na_2CO_3 in 1.00 M NaOH, and 0.25 M Na_2CO_3 in 1.00 M NaOH were exposed for the same time--one half hour. Along with these exposures an internal standard for the plate emulsion was made by exposing carbon tetrachloride for a range of times from two seconds to forty seconds with the lamp operating at 10.0 amperes. A more complete discussion of the use of an internal standard is given on page 41.

The Na_2CO_3 exposures had two purposes. The first was to quantitatively estimate the concentration of Na_2CO_3 in the hyponitrite sample (the carbonate 1065 cm^{-1} line was used for this purpose), and the second was to determine if the Na_2CO_3 could introduce any other lines besides its 1065 cm^{-1} at the concentration present in the hyponitrite sample. Using the internal standard a plot, page 25, of the concentration of Na_2CO_3 versus the equivalent time (see page 43 for an explanation of equivalent time) is shown on page 24. From this graph the estimated Na_2CO_3 concentration turns out to be about

0.80 M. Even with 1.00 M Na_2CO_3 weak lines at 692 cm^{-1} and 1115 cm^{-1} were not observable in its spectrum. If either NaNO_2 or NaNO_3 appeared as contaminants, lines should have appeared at 1331 cm^{-1} for NaNO_2 and 1055 cm^{-1} for NaNO_3 . NaNO_3 has weaker lines at 720 cm^{-1} , 1381 cm^{-1} and 1414 cm^{-1} . The absence of NaNO_2 and NaNO_3 was also confirmed by the infrared spectra.

<u>Material</u>	<u>Opacity</u>	<u>Eq. Time</u>
$\text{CO}_3^{=}\text{(N}_2\text{O}_2^{=})$	2.00	14.0
$\frac{1}{4}\text{M CO}_3^{=}$	1.23	6.0
$\frac{1}{2}\text{M CO}_3^{=}$	1.545	10.03
$1\text{M CO}_3^{=}$	2.41	16.6

The graph on page 31 shows a diagram of the infrared spectrum in the rock salt region. The $\text{Na}_2\text{N}_2\text{O}_2$ absorptions were run as Nujol mulls while the strong Na_2CO_3 absorption at 1450 cm^{-1} and the water absorptions around $3000\text{-}3600\text{ cm}^{-1}$ were run as perfluorokerosene mulls. Due to the inherent Nujol absorptions perfluorokerosene was used as a complementary mulling agent. Thus, in a perfluorokerosene mull the sample was scanned from about 1200 cm^{-1} to 1600 cm^{-1} to bring out the 1450 cm^{-1} carbonate band and from about 2800 cm^{-1} to 3600 cm^{-1} to give a clearer indication of the broad water absorption region. The diagram, of course, does not show the absorptions due to Nujol or perfluorokerosene. Thus, the absorption bands shown may be assigned as follows:

<u>Na₂N₂O₂</u>	<u>Na₂CO₃</u>	<u>H₂O</u>
630 cm ⁻¹		
867 cm ⁻¹		
	880 cm ⁻¹	
1020 cm ⁻¹	1450 cm ⁻¹	
		1690 cm ⁻¹
		3000-3600 cm ⁻¹

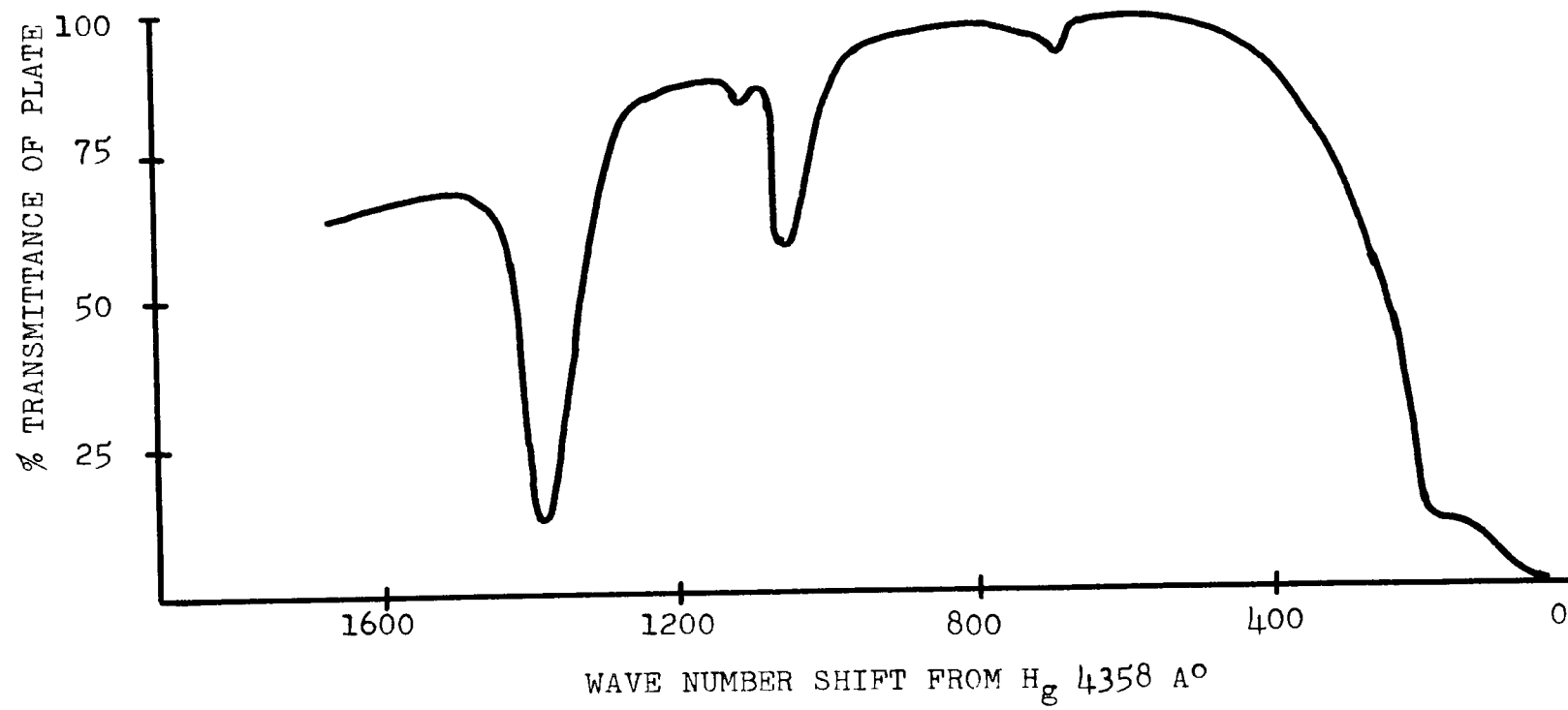
The graph on page 30 shows a drawing of the percent transmittance of the Raman plate spectrum illustrating the relative peak intensities. The scan was not carried further than about 1600 cm⁻¹ because no lines besides broad diffuse bands assignable to water or OH⁻ were observable. The line at 220 cm⁻¹ was caused by the 4358A^o H_g line. This was apparent from observation of the plate itself. Thus, the lines seen may be assigned as follows:

<u>Na₂N₂O₂</u>	<u>Na₂CO₃</u>
692 cm ⁻¹	
	1065 cm ⁻¹
1115 cm ⁻¹	
1383 cm ⁻¹	

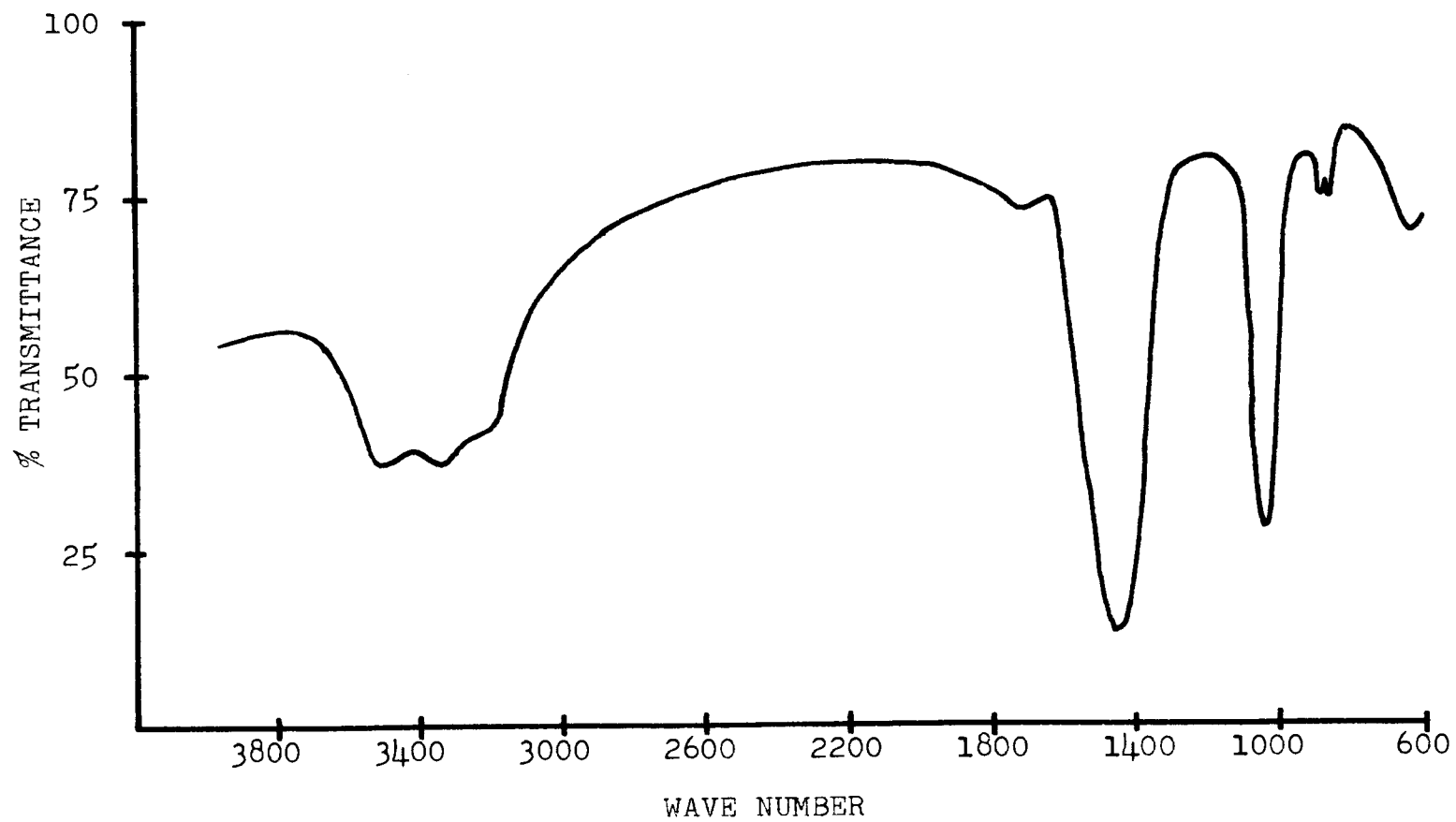
One might also suspect that the decomposition products of the hyponitrite ion could yield a sufficient concentration to give a faint Raman line. N₂O has strong lines at 1286.5 and 2223.2 cm⁻¹ (8, p. 277). Thus, dissolved gaseous N₂O could not have accounted for either

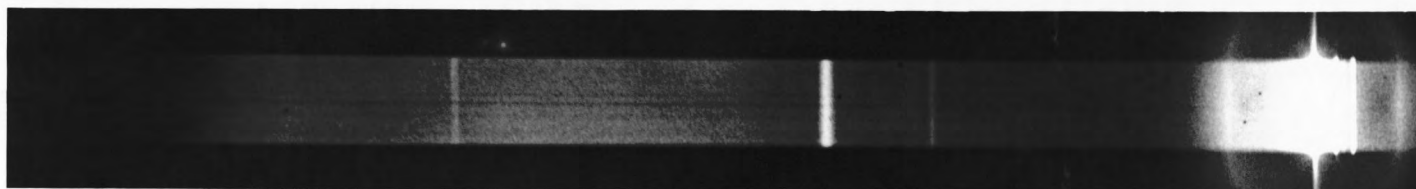
the 1115 cm^{-1} or the 692 cm^{-1} lines. Also HN_2O_2^- and $\text{H}_2\text{N}_2\text{O}_2$ could have possibly given new or shifted frequencies from those of $\text{N}_2\text{O}_2^{=}$. The addition of OH^- to the hyponitrite solution reduced drastically the concentration of these species and decreased the probability that 1115 cm^{-1} or 692 cm^{-1} could have been assigned to them. Page 32 shows a photographic reproduction of part of the plate which shows the hyponitrite ion spectrum. Also shown is the spectrum of the 1.0 M sodium carbonate and xenon and krypton reference spectra. With the xenon and krypton spectra mercury and iron lines may also be seen.

RAMAN SPECTRUM



INFRARED SPECTRUM





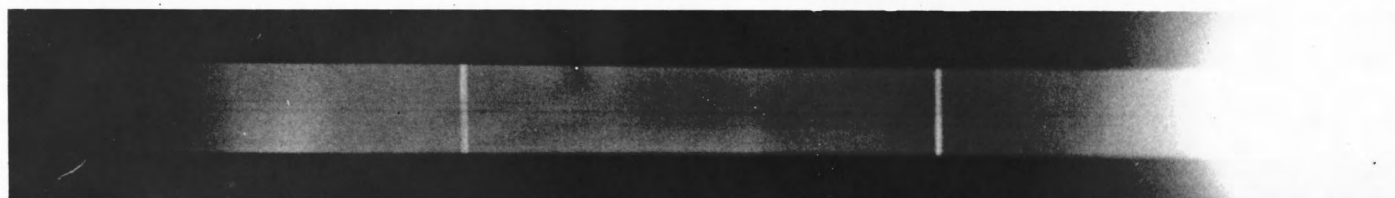
Aq. $\text{Na}_2\text{N}_2\text{O}_2$

1383 cm^{-1}

1115 cm^{-1}

692 cm^{-1}

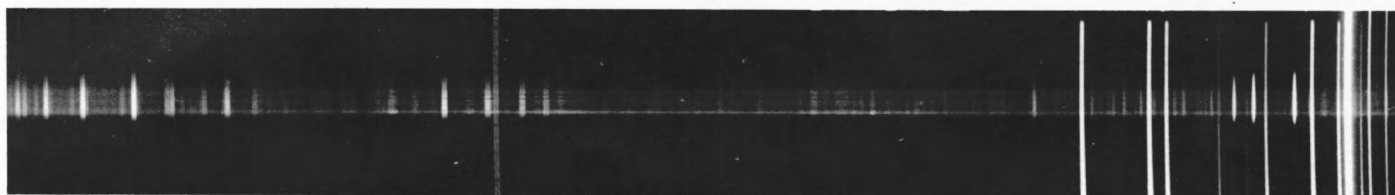
4358 Å Hg



1.0 M Na_2CO_3

1065 cm^{-1}

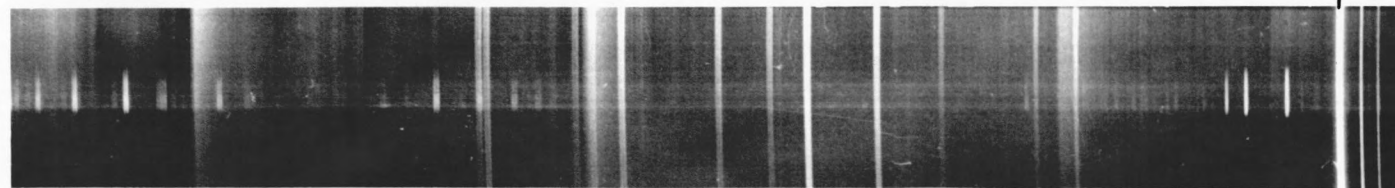
4358 Å Hg



KRYPTON

4358 Å Hg

XENON



CHAPTER V

POLARIZATION OF RAMAN LINES

A. THEORY OF THE POLARIZATION OF RAMAN LINES

The classical rate of radiation from an induced dipole per unit solid angle in the X direction is given by

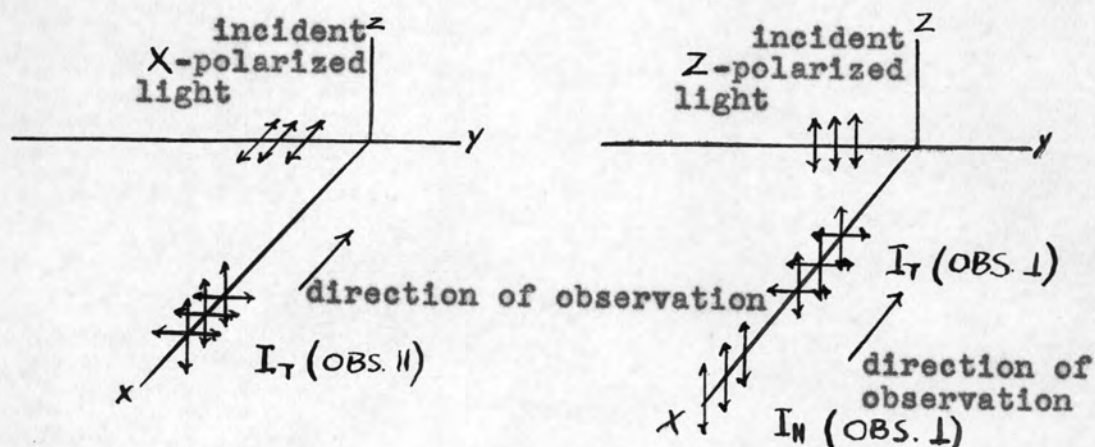
$$(1) \quad I = \frac{16\pi^4 \nu^4}{c^2} (P_{oy}^2 + P_{oz}^2) \quad (22, p. 43)$$

where ν is the frequency of oscillation and of the emitted light and P_{oy} and P_{oz} are the amplitudes in the expressions

$$(2) \quad P_y = P_{oy} \cos(2\pi\nu t + \delta)$$

$$P_z = P_{oz} \cos(2\pi\nu t + \delta')$$

P_y and P_z are components of the induced dipole. Let us now consider the case of the intensity of scattered light. Assume that the "direction of propagation of the incident light coincides with the Y axis." (22, p. 45)



I_T (obs. 11) indicates the total intensity of scattered light if the incident light is polarized parallel to the X axis. I_T (obs. \perp) indicates the total intensity of scattered light if the incident light is polarized parallel to the Z axis. And I_{11} (obs. \perp) indicates the intensity of the Z component of scattered light if the incident light is polarized parallel to the Z axis.

The depolarization ratio is "defined as the ratio of the scattered intensity which is polarized perpendicular to \vec{E} , that is, in the direction of propagation of the incident light, to the intensity parallel to \vec{E} ." (22, p. 47) "If the incident light in natural (unpolarized), the depolarization ratio may be computed by considering the scattered light to represent the sum of the intensities of the observations made parallel and perpendicular to the incident electric vector of a polarized beam. That part of the light from the parallel observation, being unpolarized, contributes one-half its intensity to the scattered light polarized, respectively, parallel and perpendicular to \vec{E} :

$$(3) \quad \rho_n = \frac{I_T(\text{OBS. } \perp) - I_{11}(\text{OBS. } \perp) + \frac{1}{2}I_T(\text{OBS. } 11)}{I_{11}(\text{OBS. } \perp) + \frac{1}{2}I_T(\text{OBS. } 11)} "$$

(22, p. 47)

In order to express ρ_n in terms of molecular parameters, let us consider a molecule acted upon by an

external light source. The induced dipole moment, \overline{P} , may be written in terms of the electric field, \overline{E} , acting on the molecule as

$$(4) \quad \overline{P} = \alpha \overline{E}$$

where α is the polarizability tensor. "It can be shown, however, that a set of axes in the molecule exists such that the relation between \overline{P} and \overline{E} , when referred to these axes, assumes the simple form

$$(5) \quad \begin{aligned} P_1 &= \alpha_1 E_1 \\ P_2 &= \alpha_2 E_2 \\ P_3 &= \alpha_3 E_3 \end{aligned} \quad \text{"} \quad (22, \text{ p. } 44)$$

Thus, according to equations (1) and (4)

$$(6) \quad \begin{aligned} I_T(\text{OBS. } \parallel) &= \frac{2\pi^3 \nu^4}{c^3} (\alpha_{yx}^2 + \alpha_{zx}^2) E_o^2 \\ I_T(\text{OBS. } \perp) &= \frac{2\pi^3 \nu^4}{c^3} (\alpha_{yz}^2 + \alpha_{zz}^2) E_o^2 \\ I_H(\text{OBS. } \perp) &= \frac{2\pi^3 \nu^4}{c^3} (\alpha_{zz}^2) E_o^2 \end{aligned}$$

Since the $\alpha_{FF'}$ refer to a laboratory fixed axis system the $\alpha_{FF'}$ should be averaged over all orientations of the molecular principal axes with respect to the fixed axes, X, Y, and Z. Since the formulas of transformation for $\alpha_{FF'}$ are of the form

$$(7) \quad \alpha_{FF'} = \sum_{i=1}^3 \alpha_i \Phi_{F1} \Phi_{F'1} \quad (22, \text{ p. } 46)$$

where the i axes refer to the principal axes of the molecule and, therefore, the quantities α_i are constants under the averaging process, the averages required are expressible as

$$(8) \overline{\alpha_{FF}^2} = \sum_i \alpha_i^2 \overline{\Phi_{Fi}^2 \Phi_{F'i}^2} + 2 \sum_{i < j} \alpha_i \alpha_j \overline{\Phi_{Fi} \Phi_{F'i} \Phi_{Fj} \Phi_{F'j}}$$

The necessary averages of the direction cosines are

$$(9) \overline{\Phi_{Fi}^2 \Phi_{F'i}^2} = \begin{cases} \frac{1}{5} & F = F' \\ \frac{1}{15} & F \neq F' \end{cases}$$

$$\overline{\Phi_{Fi} \Phi_{F'i} \Phi_{Fj} \Phi_{F'j}} = \begin{cases} \frac{1}{15} & F = F' \\ -\frac{1}{30} & F \neq F' \end{cases}$$

(22, p. 292)

Thus, for N molecules equations (6) become, using equations (8) and (9)

$$(10) \begin{aligned} I_T(\text{OBS. II}) &= \frac{1}{15} \frac{2\pi^3 \nu^4}{c^3} N E_o^2 (2 \sum_i \alpha_i^2 - 2 \sum_{i < j} \alpha_i \alpha_j) \\ I_T(\text{OBS. I}) &= \frac{1}{15} \frac{2\pi^3 \nu^4}{c^3} N E_o^2 (4 \sum_i \alpha_i^2 + \sum_{i < j} \alpha_i \alpha_j) \\ I_{11}(\text{OBS. I}) &= \frac{1}{15} \frac{2\pi^3 \nu^4}{c^3} N E_o^2 (3 \sum_i \alpha_i^2 + 2 \sum_{i < j} \alpha_i \alpha_j) \end{aligned}$$

Now if one makes the substitution of

$$(11) \quad \alpha = \frac{1}{3} (\alpha_1 + \alpha_2 + \alpha_3)$$

$$\beta^2 = \frac{1}{2} [(\alpha_1 - \alpha_2)^2 + (\alpha_2 - \alpha_3)^2 + (\alpha_3 - \alpha_1)^2]$$

where α is the spherical part of the polarizability and β is the anisotropy, equations (10) become

$$(12) \quad \begin{aligned} I_T(\text{OBS. } \parallel) &= \frac{2\pi^3\nu^4}{c^3} N E_o^2 \left(\frac{2\beta^2}{15} \right) \\ I_T(\text{OBS. } \perp) &= \frac{2\pi^3\nu^4}{c^3} N E_o^2 \left(\frac{45\alpha^2 + 7\beta^2}{45} \right) \\ I_{\parallel}(\text{OBS. } \perp) &= \frac{2\pi^3\nu^4}{c^3} N E_o^2 \left(\frac{45\alpha^2 + 4\beta^2}{45} \right) \end{aligned}$$

If now equations (12) are substituted into equation (3)

$$(13) \quad \rho_n = \frac{6\beta^2}{45\alpha^2 + 7\beta^2}$$

These results are transformed into quantum mechanical expressions by considering that the intensities will be proportional to expressions of the form

$$(14) \quad \frac{N_{n''}}{g_{n''}} \sum_{m''m'} |(\alpha_{FF'})_{m''m'}|^2 \quad (22, \text{ p. } 50)$$

where $N_{n''}$ is the number of molecules initially in the energy level described by the quantum number n'' , $g_{n''}$ is the number of degenerate initial states characterized

by the magnetic quantum number, m'' , and $(\alpha_{FF'})_{m''m'}$ is given by

$$(15) \quad (\alpha_{FF'})_{m''m'} = \int \psi_{m''}^* \alpha_{FF'} \psi_{m'} d\tau.$$

Thus, equations (12) become

$$(16) \quad I_T(\text{OBS. } \parallel) = \frac{8 \pi^3 \nu^4}{c^3} \frac{N_{n''}}{g_{n''}} E_0^2 \left(\frac{2}{15} \sum_{m''m'} \beta_{m''m'}^2 \right)$$

$$I_T(\text{OBS. } \perp) = \frac{8 \pi^3 \nu^4}{c^3} \frac{N_{n''}}{g_{n''}} E_0^2 \left(\sum_{m''m'} (\alpha_{m''m'})^2 + \frac{7}{45} \sum_{m''m'} (\beta_{m''m'})^2 \right)$$

$$I_{\parallel\parallel}(\text{OBS. } \perp) = \frac{8 \pi^3 \nu^4}{c^3} \frac{N_{n''}}{g_{n''}} E_0^2 \left(\sum_{m''m'} (\alpha_{m''m'})^2 + \frac{4}{45} \sum_{m''m'} (\beta_{m''m'})^2 \right)$$

and equation (13) becomes

$$(17) \quad \rho_n = \frac{6 \sum_{m''m'} (\beta_{m''m'})^2}{45 \sum_{m''m'} (\alpha_{m''m'})^2 + 7 \sum_{m''m'} (\beta_{m''m'})^2}.$$

It is well to note at this point that "any vibration that is antisymmetric or degenerate with respect to any other symmetry element will give a Raman line with the maximum degree of depolarization if it occurs at all"

and "therefore, only Raman lines corresponding to totally symmetric vibrations can have a degree of depolarization smaller than the maximum value $6/7$."

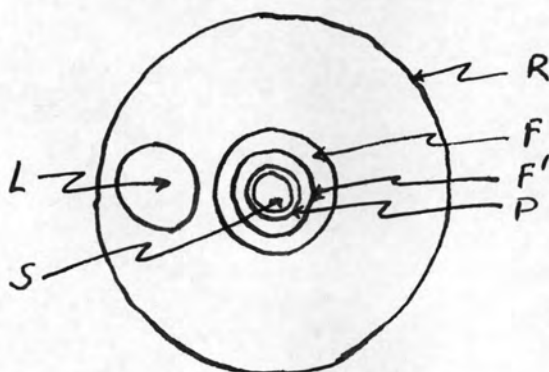
(8, p. 249) In the "cubic point groups, the totally symmetric Raman lines are completely polarized ($\rho_n = 0$)."

(8, p. 271) "For all other molecules, that is, for all non-cubic point groups, the degree of depolarization of the totally symmetric Raman lines is intermediate between 0 and $6/7$." (8, p. 271) Also one might note that the observation of the width of the Raman lines sometimes supplements the observation of their state of depolarization "When a degree of depolarization of $6/7$ is observed, for a Raman line it is probable, but not certain, that it corresponds to a non-totally symmetric vibration. Observation of a great width of the Raman line would make this certain. On the other hand, if a Raman line is quite sharp (even under fairly high dispersion) it is not certain, although probable, that the line corresponds to a totally symmetric vibration." (8, p. 491)

B. EXPERIMENTAL MEASUREMENT OF THE DEGREE OF DEPOLARIZATION OF THE 1383 cm^{-1} LINE OF $\text{Na}_2\text{N}_2\text{O}_2$

The depolarization ratio was measured, taking certain precautions, by using two polaroid cylinders, one with its polarizing axis parallel to the sample tube and the other with its axis perpendicular to the sample tube. (5, p. 124-127) The lamp, sample tube, filters, and

polaroid were placed in a cylindrical reflector coated with magnesium oxide according to the following diagram.



R is the cylindrical reflector.
 L is the low pressure H_g lamp.
 F is a one centimeter path of saturated.
 aq. NaNO₂.
 F' is a cylindrical cellophane treated
 rhodamine GDN extra.
 P is the polaroid cylinder.
 S is the sample tube.

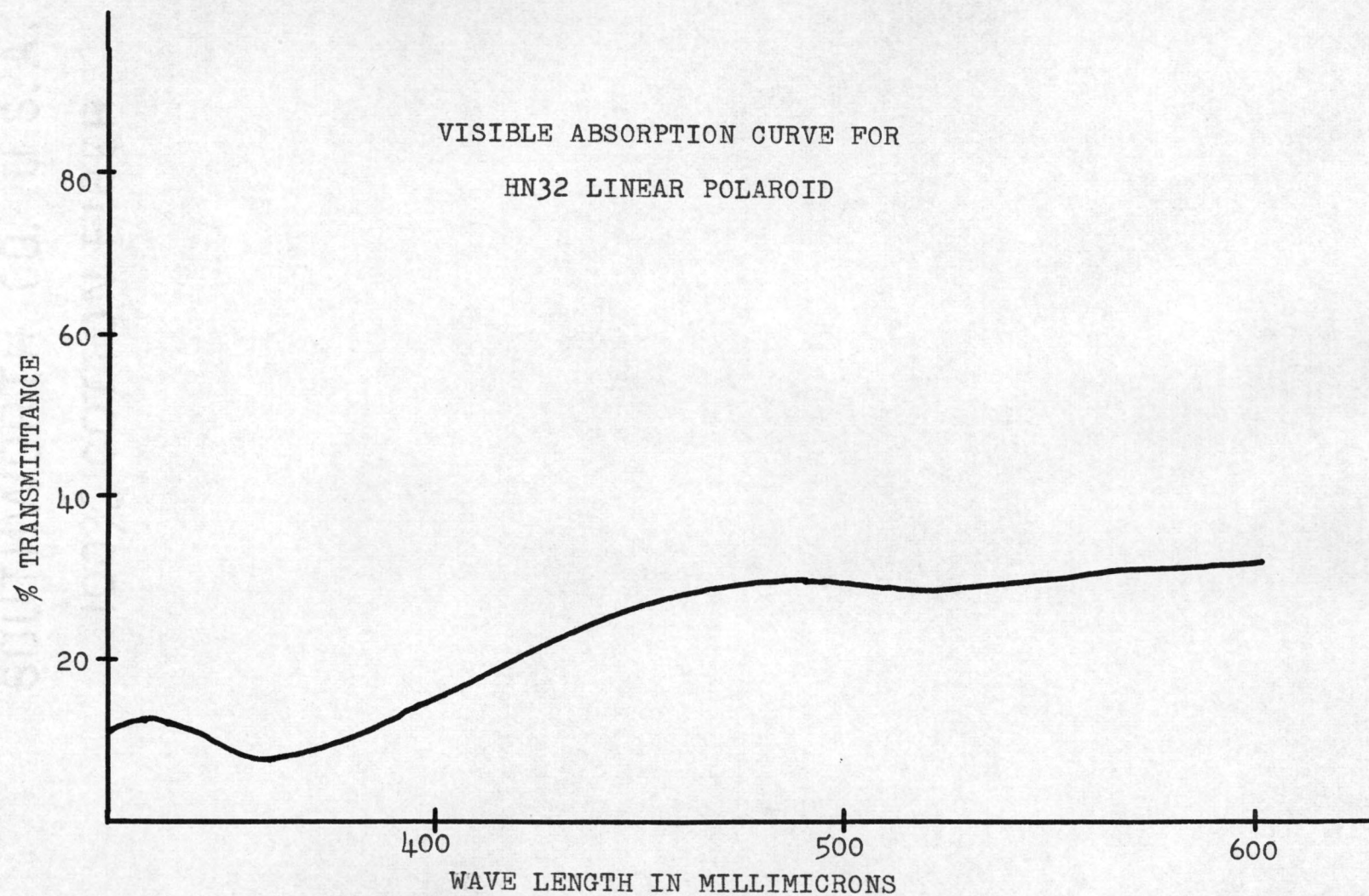
A separate discussion of the design of the apparatus concerning the low pressure H_g lamp, the light filters, and the sample tube was made in Chapter II. The polaroid used was Polaroid HN 32 plastic linear polarizer 0.010 inch in thickness of cellulose acetate butyrate purchased from the Polaroid Corporation, Cambridge 39, Mass. Its absorption curve in the visible region is shown on page 42.

The polaroid cylinder was made by wrapping the polaroid about the sample tube and uniting the two sides of the polaroid with cellophane tape. A sheet of rhodamine GDN extra treated cellophane was then wrapped about the

outside of the polaroid cylinder and again fastened with cellophane tape. The rhodamine GDN extra filter was attached permanently to the polaroid cylinder. The filter-polaroid cylinder thus made could be slid easily on or off a given sample tube.

Rank and Kagarise (19, p. 89-92) described a method in which the convergence error of such a system as this one may be corrected. However, they used a photoelectric means of detecting the spectra and did not encounter the problem of interpreting relative intensities from photographic plates. In order to attempt an interpretation from the photographic plates P_o , the observed depolarization ratio, was plotted as a function of P_t , the true or accepted value of the depolarization ratio using the following scheme for chloroform (262, 0.86; 366, 0.18; 668, 0.08), carbon tetrachloride (218, 0.83; 314, 0.82; 459, 0.044), and benzene (606, 0.8; 992, 0.04; 1177, 0.8). (4, p. 272) The first number in the series behind the given molecule represents the wave number shift of the line, and the second number gives P_t for that line.

An internal standard was produced by exposing CCl_4 from two seconds to 40 seconds. Eight different exposures of this type were made such that the logarithm of the time of exposure changed by about 0.15 units. On the same plate the required exposure was made. The zero density was taken as the region of maximum light



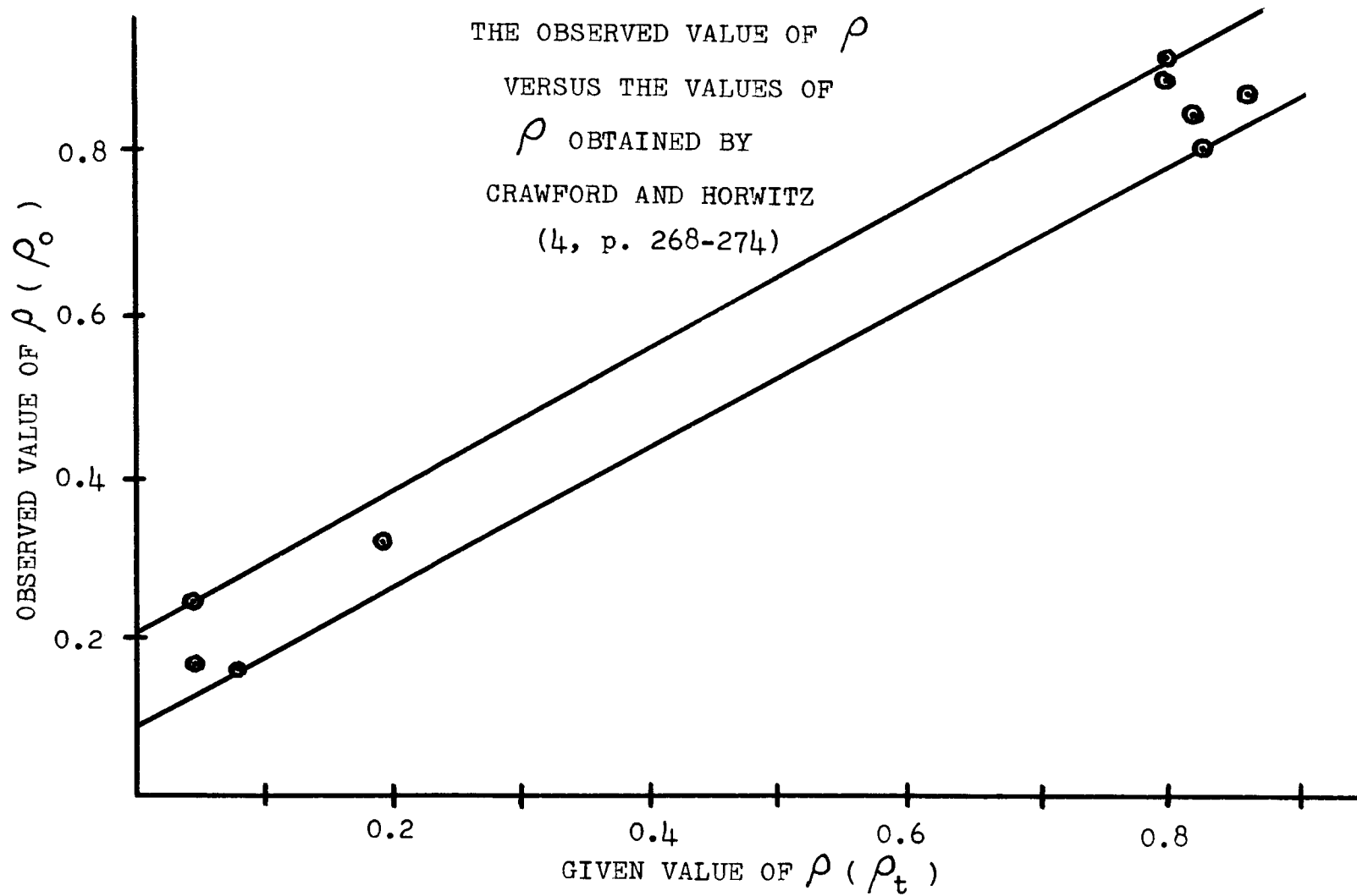
transmittance on the side of the Raman line nearer the exciting line. (4, p. 273) Thus, two exposures of the sample were taken of the same duration and identical conditions except that the polaroid cylinders were interchanged. In order to compare the intensities of a given band in the two exposures, a plot of the logarithm of the peak opacity, peak density, versus the logarithm of the time of the exposure was first plotted for the internal standard at 459 cm^{-1} (see the respective graphs for each plate). Next the logarithm of the peak opacity for the line in question in the two cases was measured. Using the calibration curve for the emulsion, these densities corresponded to two times (the equivalent times). The ratio of the time calculated for the perpendicular case to the time calculated for the parallel case was taken as the observed depolarization ratio, ρ_o .

In order to make the results have more meaning and as an attempt to correct for experimental fluctuations, such as the variable light intensity output of the H_g lamp, the calibration curve of ρ_o versus ρ_t was made from the average of six observations of each case. See the charts on pages 47, 49, and 51. Even with this method the curve came out so that one could only estimate the value of ρ_t within $\pm .08$ units. See the graph on page 46.

Three lines were observed for sodium hyponitrite: 1383 (s), 1115 (w), and 682 (vw). Although the lines at

1115 cm^{-1} and 692 cm^{-1} were visually apparent on the plate they were too weak to measure the depolarization ratio by the method employed. Besides general fogging which occurs because of light scattering from the gas bubbles upon decomposition of the hyponitrite, the line at 1115 cm^{-1} is very close to the carbonate impurity line at 1065 cm^{-1} . Because of this, only the measurement of the depolarization ratio of the line at 1383 cm^{-1} was attempted. Three exposures of about 2.5 M $\text{Na}_2\text{N}_2\text{O}_2$ with 1 M NaOH were made for each of the polaroid cylinders. Each exposure was for one hour with the lamp operating at 10.0 amperes. The average values for the opacity of the 1383 cm^{-1} line for each polaroid was calculated. The value was related to an equivalent time from the internal calibration spectra of carbon tetrachloride (page 54). The appropriate ratio of these values was taken as ρ_0 (page 53). Then from the calibration chart of ρ_0 versus ρ_t the value of ρ_t was estimated for the 1383 cm^{-1} line. ρ_0 turned out to be 0.85. Thus, ρ_t is 0.82 ± 0.08 (page 53). It is apparent that one cannot tell conclusively that ρ_t is not 6/7. The lines at 692 cm^{-1} and 1383 cm^{-1} appeared sharp. The line at 1115 cm^{-1} appeared slightly diffuse but this was not certain because the 1065 cm^{-1} line of the carbonate impurity tended to complicate this region of the spectrum.

Thus, only inconclusive information was obtainable from this approach. But it appeared probable that the lines belonged to totally symmetric modes from the apparent sharpness of the lines.



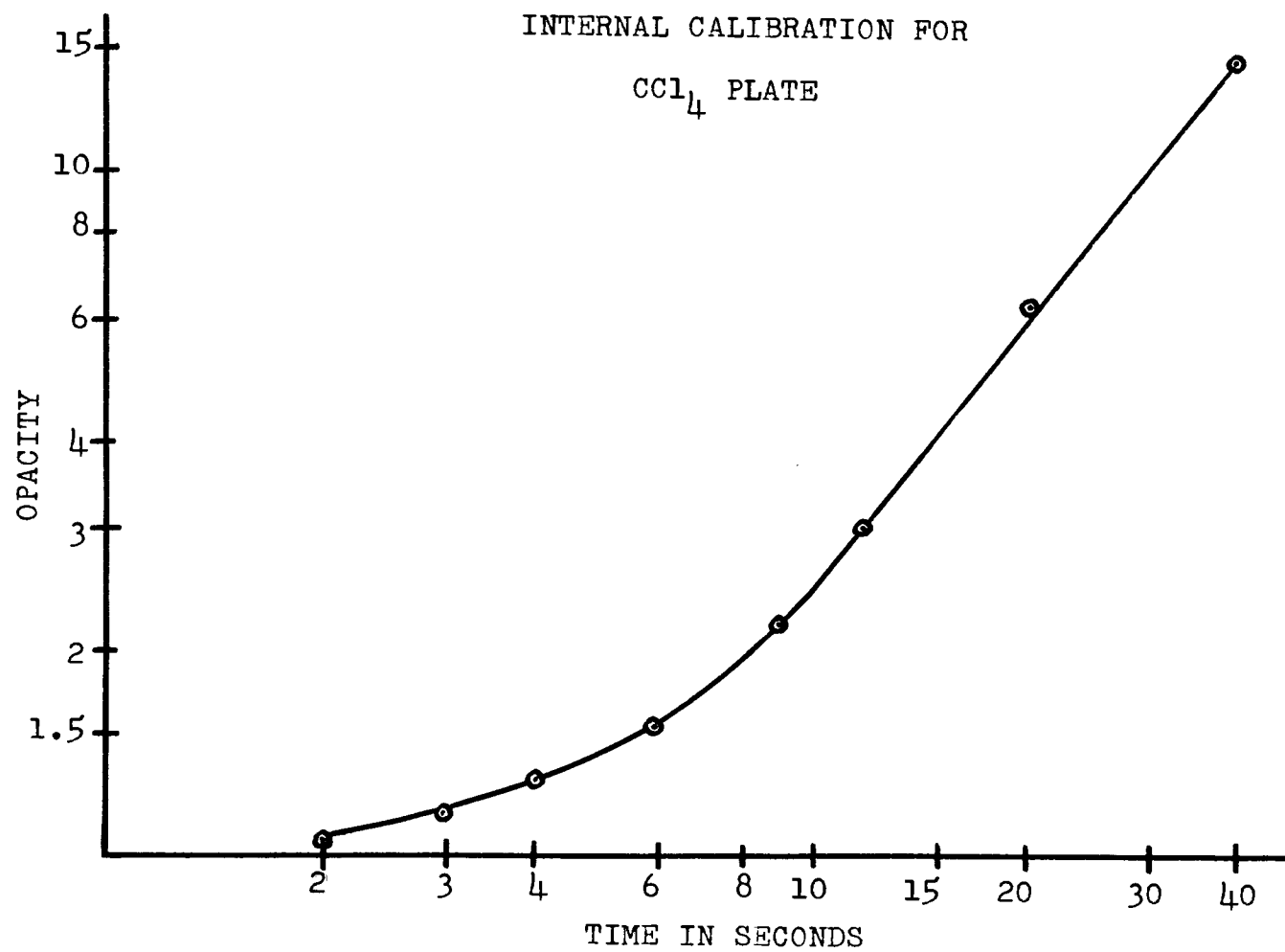
CARBON TETRACHLORIDE

Line (cm^{-1})	Opacity					Average
218	2.35	2.29	2.29	2.30	2.27	2.30
314	2.63	2.68	2.53	2.61	2.57	2.60
459	1.24	1.26	1.26	1.21	1.22	1.24

Line (cm^{-1})	⊥ Opacity						Average
218	3.25	3.16	2.94	3.00	3.02	2.89	3.04
314	3.33	3.40	3.20	3.11	3.08	3.09	3.20
459	7.48	7.64	6.97	6.82	6.61	6.42	6.99

Line (cm^{-1})	Equivalent Time	P_0	P_t *
218	9.55	.795	.83
⊥	12.0		
314	10.5	.840	.82
⊥	12.5		
459	3.75	.163	.044
⊥	23.0		

* (4, p. 268-274)



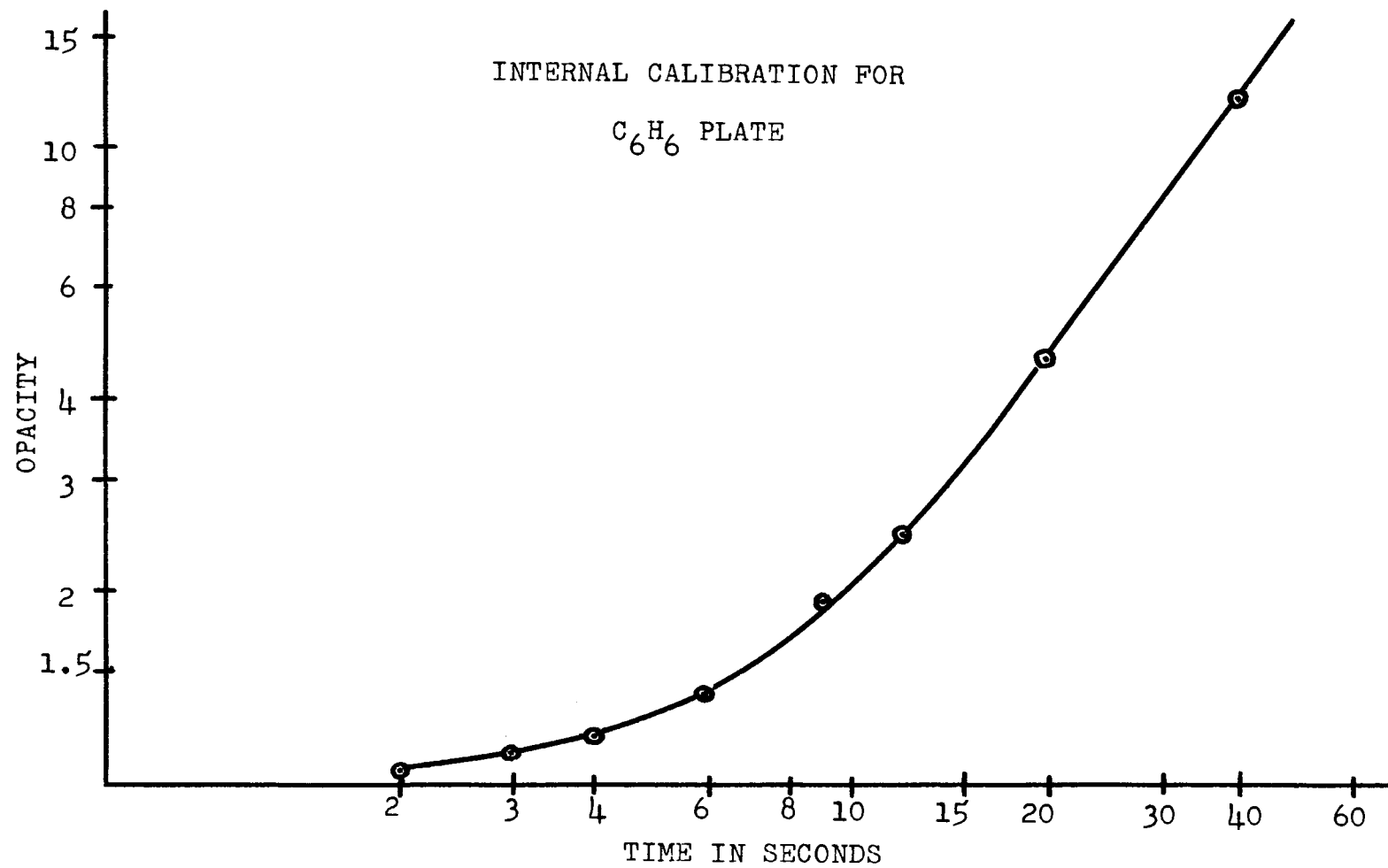
BENZENE

Line (cm^{-1})	Opacity						Average
606	1.31	1.34	1.28	1.26	1.29	1.25	1.29
992	3.00	2.97	2.91	2.90	3.05	3.12	2.99
1177	1.42	1.46	1.42	1.38	1.35	1.36	1.40

Line (cm^{-1})	\perp Opacity						Average
606	1.33	1.33	1.34	1.34	1.38	1.34	1.34
992	21.1	21.1	19.4	19.1	21.1	18.3	20.0
1177	1.50	1.50	1.52	1.50	1.45	1.44	1.48

Line (cm^{-1})	Equivalent Time	ρ_o	ρ_t *
606	5.00	.883	0.8
⊥	5.65		
992	14.3	.246	0.04
⊥	58.2		
1177	6.20	.910	0.8
⊥	6.80		

* (4, p. 268-274)



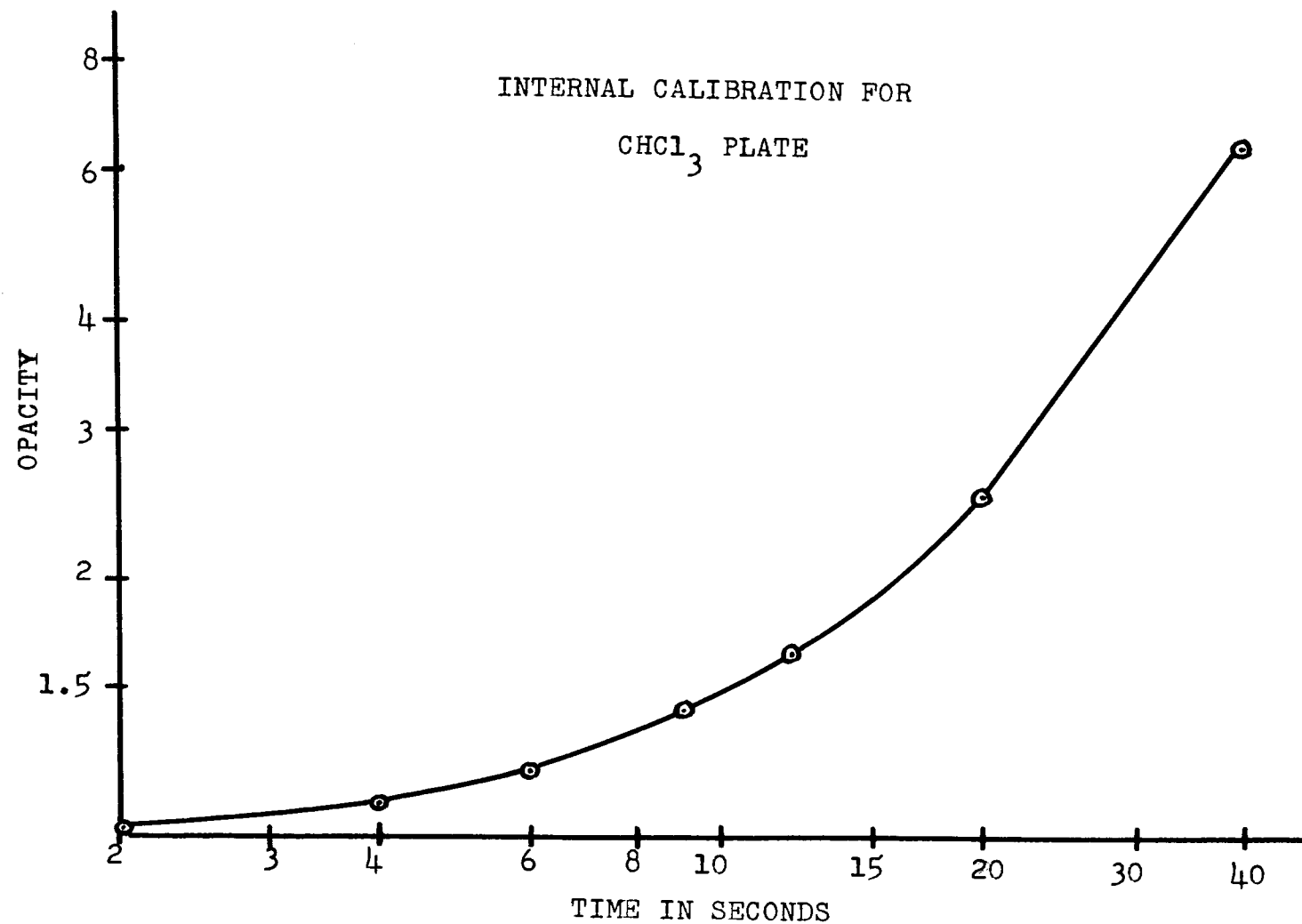
CHLOROFORM

Line (cm^{-1})	Opacity					Average
262	2.60	2.58	2.65	2.41	2.41	2.53
366	1.35	1.34	1.35	1.34	1.36	1.35
668	1.18	1.17	1.22	1.21	1.18	1.19

Line (cm^{-1})	\perp Opacity						Average
262	3.05	2.93	2.72	2.93	3.23	3.43	3.05
366	3.64	3.63	3.58	3.55	3.98	4.02	3.73
668	3.80	3.88	3.77	3.88	4.08	4.17	3.93

Line (cm^{-1})	Equivalent Time	ρ_o	ρ_t *
262	20.6	.877	.86
\perp	23.5		
366	8.50	.313	.18
\perp	27.2		
668	4.50	.154	.08
\perp	29.3		

* (4, p. 268-274)



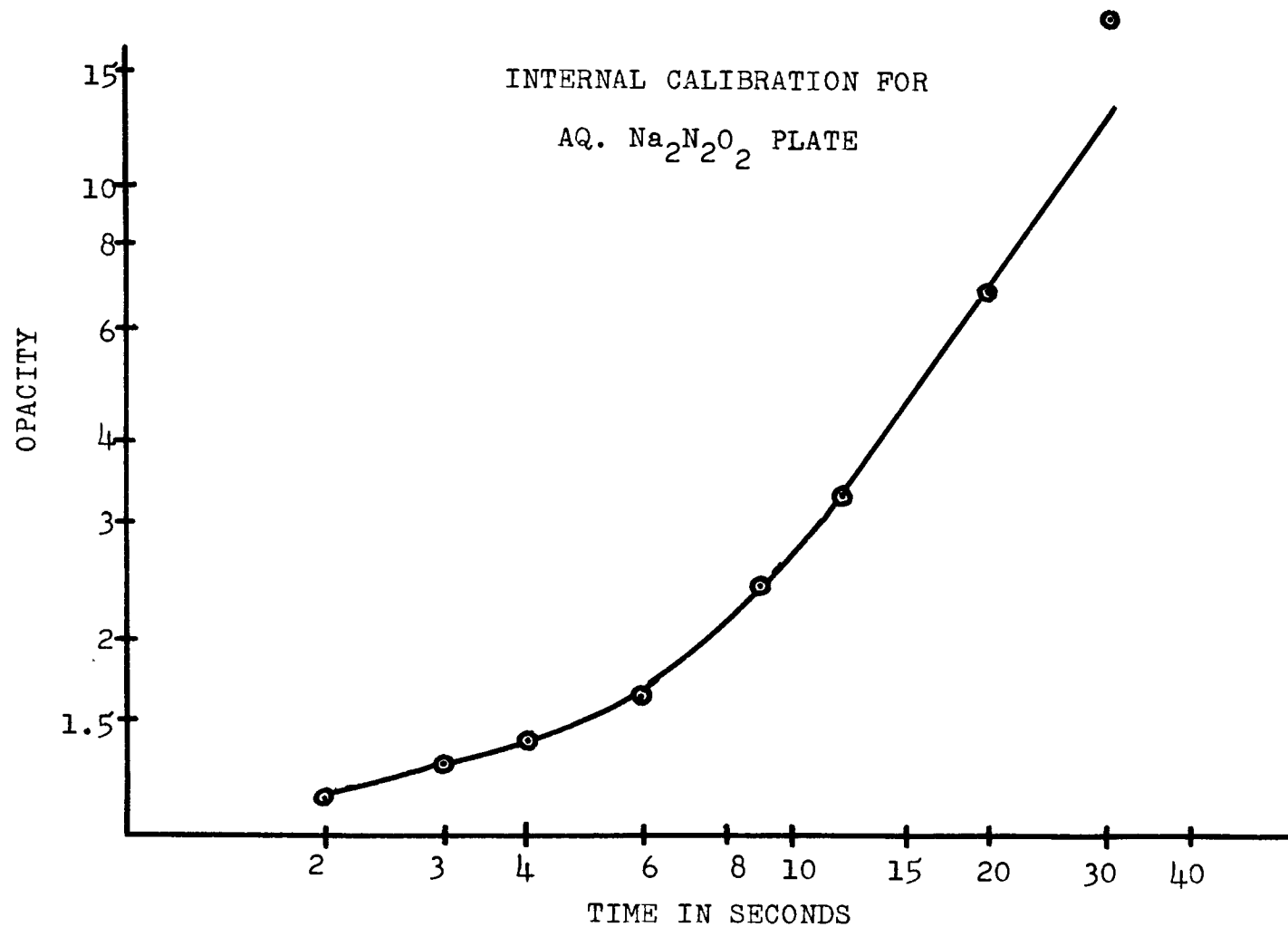
AQUEOUS SODIUM HYPONITRITE

(2-3 M)

1383 cm^{-1}

Polaroid	Opacity			Average
	4.20	3.77	3.35	3.77
⊥	4.53	4.28	5.00	4.65

Polaroid	Equivalent Time	ρ_o	ρ_t
	13.0	.848	.82 \pm .08
⊥	15.3		



CHAPTER VI

THE GF MATRIX CALCULATION OF THE FORCE CONSTANTS
OF THE HYPONITRITE ION

Let

$$(17) \quad G_{tt'} = \sum_{\alpha=1}^N \mu_{\alpha} \bar{s}_{t\alpha} \cdot \bar{s}_{t'\alpha} \quad (22, \text{ p. 61})$$

where $\bar{s}_{t\alpha}$ is defined as follows: "The direction of $\bar{s}_{t\alpha}$ is the direction in which a given displacement of atom α will produce the greatest increase of S_t . The magnitude of $\bar{s}_{t\alpha}$ is equal to the increase of S_t produced by a unit displacement of the atom α in this most effective direction." (22, p. 55) The quantity μ_{α} is the reciprocal mass of atom α . Then it can be shown "that the kinetic energy of vibration can be written in terms of internal coordinates in the form

$$(18) \quad 2T = \sum_{tt'} (G^{-1})_{tt'} \dot{S}_t \dot{S}_{t'} \quad (22, \text{ p. 63})$$

where the matrix G^{-1} is the inverse of G . "If the potential energy is expressed in the same internal coordinates so that

$$(19) \quad 2V = \sum_{tt'} F_{tt'} S_t S_{t'},$$

$F_{tt'}$ being the force constants, the vibrational problem leads to a secular equation" (22, p. 64)

$$(20) \quad |F - G^{-1}\lambda| = 0$$

where $\lambda = 4\pi^2\nu^2$ and the determinant has n rows and n columns. n is the number of internal coordinates. Thus, if equation (20) is multiplied by the determinant of the matrix G the final result is

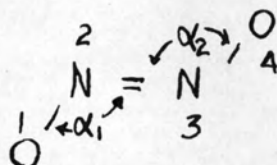
$$(21) \quad |GF - E\lambda| = 0$$

or

$$(22) \quad |FG - E\lambda| = 0$$

since F and G are both symmetrical matrices.

Now, consider the hyponitrite ion for which the structure has been proposed to be C_{2h} . (9, p. 1820-1821) (For a discussion which discounts some other possible structures see Millen, et al.'s paper (12, p. 687-691).)



Let the internal coordinates be defined in terms of the above diagram by

$$(23) \quad \begin{aligned} s_1 &= r_{23} = r_1 \\ s_2 &= r_{12} = r_2 \\ s_3 &= r_{34} = r_3 \end{aligned}$$

(23 continued)

$$s_4 = \sqrt{r_{12}r_{23}} \alpha_1$$

$$s_5 = \sqrt{r_{34}r_{23}} \alpha_2$$

Then the \bar{s}_{tt} vectors may be written as follows: ($\bar{e}_{\alpha\alpha'}$ is a unit vector from atom α to atom α' .)

$$(24) \quad \begin{array}{lll} \bar{s}_{11} = 0 & \bar{s}_{21} = \bar{e}_{21} & \bar{s}_{31} = 0 \\ \bar{s}_{12} = \bar{e}_{32} & \bar{s}_{22} = -\bar{e}_{21} & \bar{s}_{32} = 0 \\ \bar{s}_{13} = -\bar{e}_{32} & \bar{s}_{23} = 0 & \bar{s}_{33} = -\bar{e}_{34} \\ \bar{s}_{14} = 0 & \bar{s}_{24} = 0 & \bar{s}_{34} = \bar{e}_{34} \end{array}$$

$$\bar{s}_{41} = \sqrt{\frac{r_{23}}{r_{12}}} \left(\frac{\bar{e}_{21} \cos \alpha_1 + \bar{e}_{32}}{\sin \alpha_1} \right)$$

$$\bar{s}_{42} = -\sqrt{\frac{r_{23}}{r_{12}}} \left(\frac{\bar{e}_{21} \cos \alpha_1 + \bar{e}_{32}}{\sin \alpha_1} \right) - \sqrt{\frac{r_{12}}{r_{23}}} \left(\frac{-\bar{e}_{32} \cos \alpha_1 - \bar{e}_{21}}{\sin \alpha_1} \right)$$

$$\bar{s}_{43} = \sqrt{\frac{r_{12}}{r_{23}}} \left(\frac{-\bar{e}_{32} \cos \alpha_1 - \bar{e}_{21}}{\sin \alpha_1} \right)$$

$$\bar{s}_{44} = 0$$

$$\bar{s}_{51} = 0$$

$$\bar{s}_{52} = -\sqrt{\frac{r_{34}}{r_{23}}} \left(\frac{\bar{e}_{32} \cos \alpha_2 - \bar{e}_{34}}{\sin \alpha_2} \right)$$

(24 continued)

$$\bar{s}_{53} = -\sqrt{\frac{r_{34}}{r_{23}}} \left(\frac{\bar{e}_{32} \cos \alpha_2 - \bar{e}_{34}}{\sin \alpha_2} \right) - \sqrt{\frac{r_{23}}{r_{34}}} \left(\frac{\bar{e}_{34} \cos \alpha_2 - \bar{e}_{32}}{\sin \alpha_2} \right)$$

$$\bar{s}_{54} = \sqrt{\frac{r_{23}}{r_{34}}} \left(\frac{\bar{e}_{34} \cos \alpha_2 - \bar{e}_{32}}{\sin \alpha_2} \right)$$

Thus, the G matrix for the hyponitrite ion may be constructed from equation (17) and equations (24)

$$(25) \quad G_{11} = \frac{1}{m_2} + \frac{1}{m_3}$$

$$G_{12} = \frac{\cos \alpha_1}{m_2}$$

$$G_{13} = \frac{\cos \alpha_2}{m_3}$$

$$G_{14} = -\sqrt{\frac{r_{23}}{r_{12}}} \frac{\sin \alpha_1}{m_2}$$

$$G_{15} = -\sqrt{\frac{r_{23}}{r_{34}}} \frac{\sin \alpha_2}{m_3}$$

$$G_{22} = \frac{1}{m_1} + \frac{1}{m_2}$$

$$G_{23} = 0$$

(25 continued)

$$G_{24} = -\sqrt{\frac{r_{12}}{r_{23}}} \frac{\sin \alpha_1}{m_2}$$

$$G_{25} = -\sqrt{\frac{r_{34}}{r_{23}}} \frac{\sin \alpha_2}{m_3}$$

$$G_{33} = \frac{1}{m_3} + \frac{1}{m_4}$$

$$G_{34} = -\sqrt{\frac{r_{12}}{r_{23}}} \frac{\sin \alpha_1}{m_3}$$

$$G_{35} = -\sqrt{\frac{r_{34}}{r_{23}}} \frac{\sin \alpha_2}{m_3}$$

$$G_{44} = \frac{r_{23}}{r_{12}} \left(\frac{1}{m_1} + \frac{1}{m_2} \right) + \frac{r_{12}}{r_{23}} \left(\frac{1}{m_3} + \frac{1}{m_2} \right) - \frac{2\cos\alpha}{m_2}$$

$$G_{45} = \frac{r_{12}}{r_{23}} \left(\frac{1}{m_2} + \frac{1}{m_3} \right) - \cos\alpha \left(\frac{1}{m_2} + \frac{1}{m_3} \right)$$

$$G_{55} = \frac{r_{34}}{r_{23}} \left(\frac{1}{m_2} + \frac{1}{m_3} \right) + \frac{r_{23}}{r_{34}} \left(\frac{1}{m_4} + \frac{1}{m_3} \right) - \frac{2\cos\alpha}{m_3}$$

$$r_{12} = r_{34}$$

$$\alpha_1 = \alpha_2$$

$$m_1 = m_4$$

$$m_2 = m_3$$

Now in terms of these internal coordinates the potential energy may be written as

$$\begin{aligned}
 (26) \quad 2V = & F_R s_1^2 + F_r (s_2^2 + s_3^2) + F_\alpha (s_4^2 + s_5^2) \\
 & + 2F_{R\alpha} (s_1 s_4 + s_1 s_5) + 2F_{r\alpha} (s_2 s_4 + s_3 s_5) \\
 & + 2F_{r'\alpha} (s_2 s_5 + s_3 s_4) + 2F_{Rr} (s_1 s_2 + s_1 s_3) \\
 & + 2F_{rr} (s_2 s_3) + 2F_{\alpha\alpha} (s_4 s_5)
 \end{aligned}$$

or

$$(27) \quad F = \begin{pmatrix} F_R & F_{Rr} & F_{Rr} & F_{R\alpha} & F_{R\alpha} \\ & F_r & F_{rr} & F_{r\alpha} & F_{r'\alpha} \\ & & F_r & F_{r'\alpha} & F_{r\alpha} \\ & & & F_\alpha & F_{\alpha\alpha} \\ & & & & F_\alpha \end{pmatrix}$$

In order to simplify the form of the GF matrix the F and G matrices which have been found will be transformed to correspond with a set of internal symmetry coordinates.

(22, p. 117) Hence, let

$$(28) \quad s^{(\gamma)} = N \sum_R \chi_R^{(\gamma)} s_{R1}$$

where $s^{(\gamma)}$ is a symmetry coordinate, N is a normalizing

factor, $\chi_R^{(\gamma)}$ is the character for a given species and symmetry operation, and RS_1 "stands for the coordinate to which the displacement of S_1 is transferred by the operation R." (22, p. 119) Using this procedure the symmetry coordinates for this ion are

$$\begin{aligned}
 (28) \quad S_R^{(Ag)} &= R \\
 S_r^{(Ag)} &= \frac{1}{\sqrt{2}} (r_1 + r_2) \\
 S_\alpha^{(Ag)} &= \frac{1}{\sqrt{2}} (\alpha_1 + \alpha_2) \\
 S_r^{(Bu)} &= \frac{1}{\sqrt{2}} (r_1 - r_2) \\
 S_\alpha^{(Bu)} &= \frac{1}{\sqrt{2}} (\alpha_1 - \alpha_2)
 \end{aligned}$$

Next the G and F matrices will be transformed to correspond to these symmetry coordinates.

This is accomplished by the rule for diagonal constants: "Multiply the force constant in the first row and in the column labeled by a given internal coordinate by the coefficient with which that internal coordinate appears in the symmetry coordinate. Then divide by the coefficient of the first internal coordinate (row label). Do this for each column and add the results." (22, p. 130) And for off diagonal constants: "Multiply the force constants in the first row and in the column labeled by a given internal coordinate by the coefficient with which

that internal coordinate appears in the symmetry coordinate. Then divide by the coefficient of the first internal coordinate of the other set (row label). Do this for each column and add." (22, p. 131) Using these rules the G and F matrices become

$$(29) \quad G^{(Ag)} = \begin{pmatrix} G_{11} & \frac{1}{\sqrt{2}}(G_{12} + G_{13}) & \frac{1}{\sqrt{2}}(G_{14} + G_{15}) \\ & G_{22} + G_{23} & G_{24} + G_{25} \\ & & G_{44} + G_{45} \end{pmatrix}$$

$$F^{(Ag)} = \begin{pmatrix} F_R & \sqrt{2}F_{Rr} & \sqrt{2}F_R \\ & F_r + F_{rr} & F_{r\alpha} + F_{r\alpha}' \\ & & F_{\alpha} + F_{\alpha\alpha} \end{pmatrix}$$

$$G^{(Bu)} = \begin{pmatrix} G_{22} - G_{23} & G_{24} - G_{25} \\ & G_{44} - G_{45} \end{pmatrix}$$

$$F^{(Bu)} = \begin{pmatrix} F_r - F_{rr} & F_{r\alpha} - F_{r\alpha}' \\ & F_{\alpha} - F_{\alpha\alpha} \end{pmatrix}$$

However, it was shown in equations (25) that $G_{12} = G_{13}$, $G_{14} = G_{15}$, $G_{23} = 0$, and $G_{24} = G_{25}$. Thus,

$$(30) \quad G^{(Ag)} = \begin{pmatrix} G_{11} & \sqrt{2} G_{12} & \sqrt{2} G_{14} \\ & G_{22} & 2G_{24} \\ & & G_{44} + G_{45} \end{pmatrix}$$

and

$$G^{(Bu)} = \begin{pmatrix} G_{22} & 0 \\ & G_{44} - G_{45} \end{pmatrix}$$

Next let us tabulate the components of the GF matrix.

(31)

$$(GF)_{11} = G_{11}F_R + 2G_{12}F_{Rr} + 2G_{14}F_{R\alpha}$$

$$(GF)_{12} = \sqrt{2}G_{11}F_{Rr} + \sqrt{2}G_{12}(F_r + F_{rr}) + \sqrt{2}G_{14}(F_\alpha + F'_{r\alpha})$$

$$(GF)_{13} = \sqrt{2}G_{11}F_{R\alpha} + \sqrt{2}G_{12}(F_{r\alpha} + F'_{r\alpha}) + \sqrt{2}G_{14}(F_\alpha + F_{\alpha\alpha})$$

$$(GF)_{22} = 2G_{12}F_{Rr} + G_{22}(F_r + F_{rr}) + 2G_{24}(F_{r\alpha} + F'_{r\alpha})$$

$$(GF)_{23} = 2G_{12}F_{R\alpha} + G_{22}(F_{r\alpha} + F'_{r\alpha}) + 2G_{24}(F_\alpha + F_{\alpha\alpha})$$

$$(GF)_{33} = 2G_{14}F_{R\alpha} + 2G_{24}(F_{r\alpha} + F'_{r\alpha}) + (G_{44} + G_{45})(F_\alpha + F_{\alpha\alpha})$$

$$(GF)_{44} = G_{22}(F_r - F_{rr})$$

$$(GF)_{45} = G_{22}(F_{r\alpha} - F'_{r\alpha})$$

$$(GF)_{55} = (G_{44} - G_{45})(F_\alpha - F_{\alpha\alpha})$$

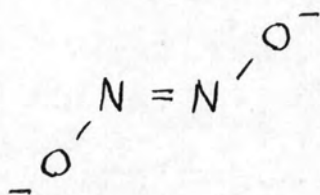
If $F_{r\alpha}^i$, F_{rr} , and $F_{\alpha\alpha}$ are neglected, being considered insignificant, there are two bond distances (r_1 and r_2), one angle (α), one angle force constant (F_α), two major bond force constants (F_R and F_r), one bond-bond interaction force constant (F_{Rr}), and two bond-angle interaction force constants ($F_{R\alpha}$ and $F_{r\alpha}$) to determine from the known data neglecting the out of plane distortion force constant. Thus, if two infrared Bu vibrational frequencies are known the problem is underdetermined, since for the five vibrational frequencies there are nine parameters to determine. Hence, it is easy to see that exact values or even correct values for the force constants will be difficult to calculate. However, intuition may be used to obtain a reasonable estimate of the free constants. First, the bond angle, α , may be guessed to be near 120° if the hyponitrite ion has C_{2h} symmetry. Second, the unknown parameters may be reduced to eight, since only the ratio of the bond distances (r_2/r_1) occurs in the FG matrix. Third, a value of r_2/r_1 may be estimated from the observed values of the N-O and N-N distances in other molecules. In light of these remarks the calculation will be continued in such a manner as to assign reasonable values to α and r_2/r_1 , and then determine F_r , F_α , F_{Rr} , F_R , and $F_{R\alpha}$ as a function of $F_{r\alpha}$.

The following table lists the values of several bonds which have similarities to the bonds of the hyponitrite ion.

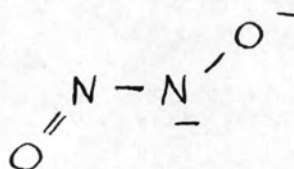
Table of Bond Lengths

<u>Bond</u>	<u>Molecule</u>	<u>Distance (\AA)</u>	<u>Reference</u>
N-O	NH ₂ OH	1.46	6, p. 147
N \equiv O	NNO	1.191	3, p. 178
N \equiv O	NO ₂	1.19	20, p. 1248-1251
N=O	ONF	1.13	10, p. 1071
N=O	NO ₂ ⁻	1.13	13, p. 444-446
N-N	N ₂ H ₄	1.47 \pm .02	17, p. 228
N \equiv N"	HN'N"N"	1.240 \pm .003	1, p. 1422
N \equiv N"	HN'N"N"	1.134 \pm .003	1, p. 1422
N \equiv N	NNO	1.126	2, p. 72; 3, p. 178

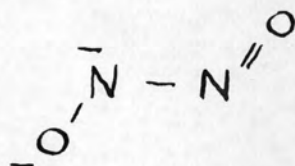
In order to compare the bonds in the preceeding table with those of the hyponitrite ion, something must be said on the type of bonds expected in the hyponitrite ion. The structure which is considered dominant by considerations of the C_{2h} symmetry is



But, structures such as



and



may also play a significant role in the ion's structure. One may make an estimate of the ratio of the bond distances, r_2/r_1 by assigning to r_2 the N-O bond distance of NH_2OH and to r_1 the $\text{N}'\equiv\text{N}''$ bond distance of $\text{HN}'\text{N}''\text{N}'''$. Thus, r_2/r_1 becomes 1.176. The value of the ratio is only an estimate and it cannot be considered as the correct value to use. However, this does give a starting point for the calculations, and on page 81 reasoning is given for the selection of 1.135 as the value for the ratio of the bond distances.

Next, in order to assess a logical assignment of the fundamental vibrational frequencies, the assignment of the vibrational frequencies previously published and those which I have reported in the previous sections will be compared. Kuhn and Lippincott (9, p. 1820-1821) have reported the following values for the infrared and Raman spectra of the hyponitrite ion.

<u>IR (ω cm⁻¹)</u>	<u>RAMAN ($\Delta \omega$ cm⁻¹)</u>	<u>ASSIGNMENT</u>
. 1392		N=N stretch
1090		
1035 mwantisym. N-O stretch
. 958		sym. N-O stretch
885 w		
629 m		NNO bend
492 w		ONNO distortion

Millen, Polydoropoulos, and Watson (13, p. 687-691) have also reported values for the Raman and infrared spectra of the hyponitrite ion.

<u>IR (ω cm⁻¹)</u>	<u>RAMAN ($\Delta \omega$ cm⁻¹)</u>	<u>ASSIGNMENT</u>
2207		$\nu_2 + \nu_5$ Bu
. 1383		ν_1 Ag
1129		$2\nu_4 + \nu_6$ Au
1020		ν_5 Bu
. 1115		ν_2 Ag
863		$\nu_3 + \nu_4$ Bu
504		ν_6 Au
. (485)		ν_3 Ag
(370)		ν_4 Bu

In comparison with these two papers I have found the following spectra to be consistent with my observations.

<u>IR ($\omega_{\text{cm}^{-1}}$)</u>	<u>RAMAN ($\Delta\omega_{\text{cm}^{-1}}$)</u>	<u>ASSIGNMENT</u>	
. 1383s	N=N stretch	ν_1	
. 1115wsym. N-O stretch	ν_2	
1020s.antisym. N-O stretch	ν_4	
885 w			
. 692w	sym. NNO bend	ν_3	
629 m	ONNO distortion	ν_6	
492 w	NNO bend	ν_5	

The 492 cm^{-1} band was observed in connection with another study being carried on at Oregon State University. This band was observed as a broad band somewhere in the vicinity of $480\text{-}495 \text{ cm}^{-1}$.

Now, from $\nu_1, \nu_2, \nu_3, \nu_4$, and ν_5 the required $\lambda_1, \lambda_2, \lambda_3, \lambda_4$, and λ_5 may be evaluated from the expression given on page . Hence,

$$(32) \quad \lambda = 4\pi^2\nu^2 = 4\pi^2c^2\omega^2 = \left(\frac{\omega}{1303.1}\right)^2$$

where the last form is consistent with the following system of units: masses in atomic weight units, lengths in angstroms, and the force constants in $10^5 \text{ dynes cm}^{-1}$.

The results may be summarized in the following table:

ν	ω (cm ⁻¹)	λ
ν_1	1383	1.125
ν_2	1115	.726
ν_3	692	.285
ν_4	1020	.6126
ν_5	492	.1426

In a consideration of the B_u species part of the FG matrix it was found that only r_2/r_1 , F_α , F_r , and $F_{r\alpha}$ need be considered. From this view point then F_α and F_r may be expressed as a function of $F_{r\alpha}$ for a given value of r_2/r_1 . From equations (31) the B_u part of the secular determinant becomes

$$(33) \quad \begin{vmatrix} G_{22}F_r - \lambda & G_{22}F_{r\alpha} \\ G_{22}F_{r\alpha} & (G_{44} - G_{45})F_\alpha - \lambda \end{vmatrix} = 0$$

Hence, for ν_4 and ν_5

$$(34) \quad F_\alpha = \frac{\lambda_4 + \lambda_5 \pm \sqrt{(\lambda_4 + \lambda_5)^2 - 4(\lambda_4\lambda_5 + G_{22}^2 F_{r\alpha}^2)}}{2(G_{44} - G_{45})}$$

and

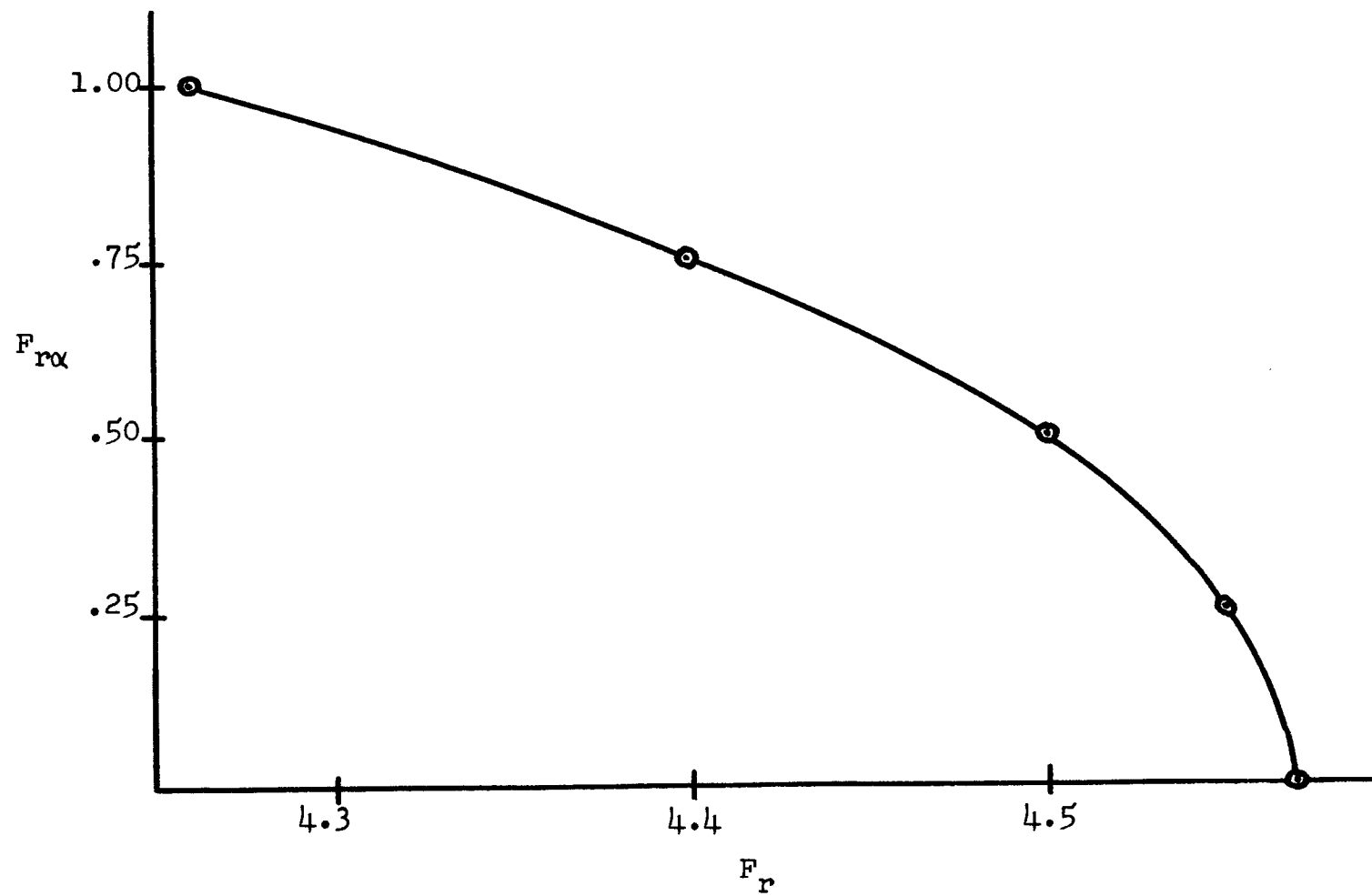
$$(35) \quad F_r = \frac{\lambda_4 + \lambda_5 \pm \sqrt{(\lambda_4 + \lambda_5)^2 - 4(\lambda_4\lambda_5 + G_{22}^2 F_{r\alpha}^2)}}{2G_{22}}$$

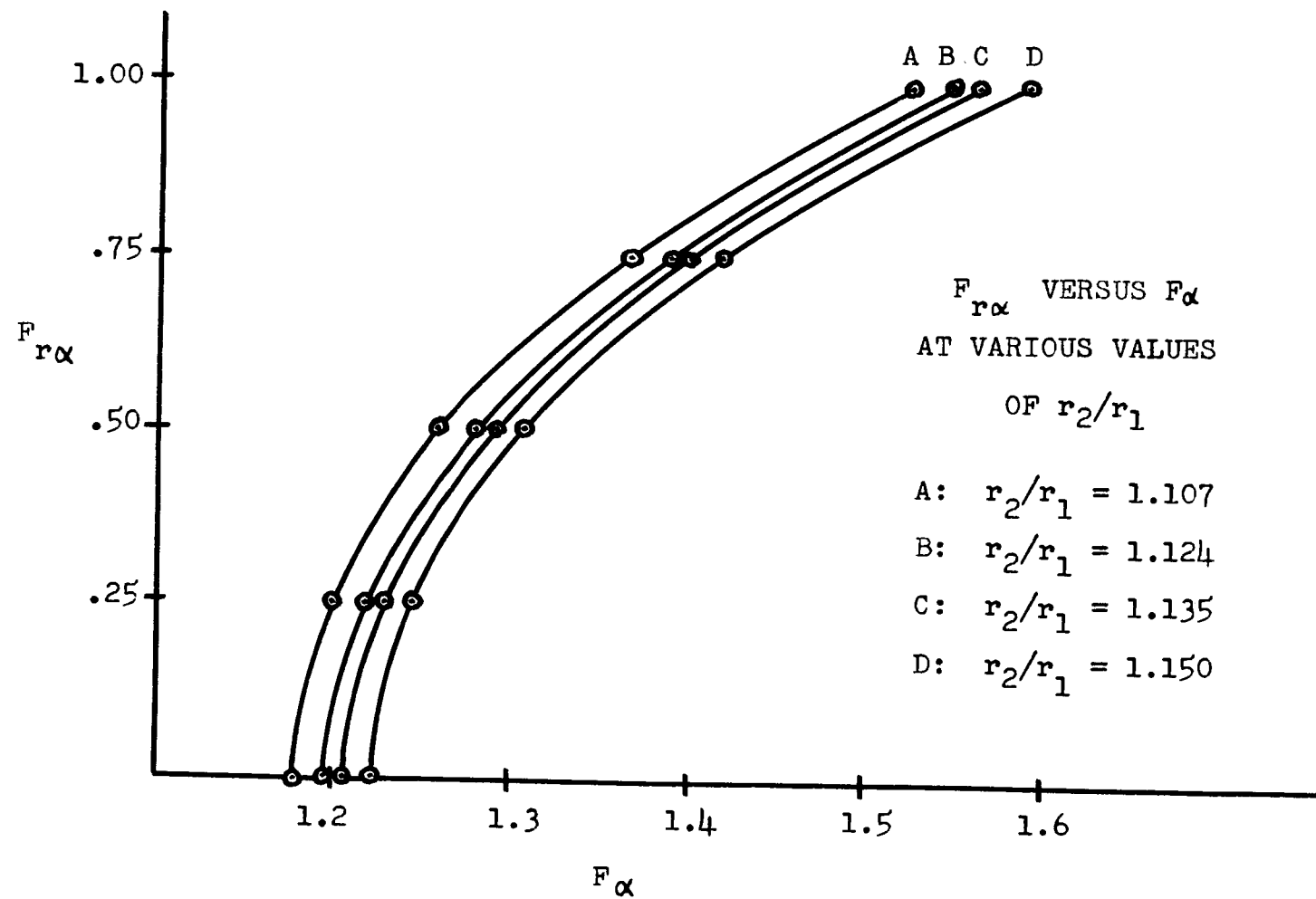
Since G_{22} is only a function of the masses of the nitrogen and oxygen atoms, F_r is also independent of r_2/r_1 . Since equations (34) and (36) would give two sets of solutions for each value of $F_{r\alpha}$, a selection must be made as to which is the most appropriate solution. For comparison let us select $F_{r\alpha} = 0$ and $r_2/r_1 = 1.135$. First, select the negative sign before the square root symbol in equation (34). This means that the corresponding solution in equation (35) is given by using the positive sign before the square root symbol in this equation. Hence, $F_r = 4.57$ and $F_\alpha = 1.205$. The other set of solutions is obtained by reversing the signs before the square root symbols in the two equations. Hence, F_r now becomes 1.06 and F_α equals 5.18. One can conclude from this that the negative sign must be used in equation (34) and the positive sign in equation (35) because 5.18 is extremely large for a bending force constant such as F_α and 1.06 is extremely small for a bond force constant such as F_r . The results for a set of selected values of r_2/r_1 are given next and graphed on pages 72 and 73. The force constants are in 10^5 dynes/cm.

$\frac{F_{r\alpha}}{r}$	$\frac{F_r}{r}$
0	4.57
.25	4.55
.50	4.50
.75	4.40
1.00	4.26

$\frac{r_2}{r_1}$	$\frac{F_{r\alpha}}{r}$	$\frac{F\alpha}{r}$
1.107	0	1.177
	.25	1.198
	.50	1.258
	.75	1.365
	1.00	1.522
1.124	0	1.196
	.25	1.218
	.50	1.280
	.75	1.388
	1.00	1.548
1.135	0	1.205
	.25	1.228
	.50	1.291
	.75	1.400
	1.00	1.561
1.150	0	1.221
	.25	1.245
	.50	1.307
	.75	1.418
	1.00	1.580

$F_{r\alpha}$ VERSUS F_r





In using the Ag species part of the secular determinant simple expressions giving $F_{R\alpha}$, F_{Rr} , and F_R in terms of F_α , F_r , and $F_{r\alpha}$ are not easily found. Because of this difficulty a different procedure will be outlined whereby the values of $F_{R\alpha}$, F_{Rr} , and F_R may be evaluated.

The expressions for the components of the GF matrix are

$$\begin{aligned}
 (36) \quad (GF)_{11} &= G_{11}F_R + 2G_{12}F_{Rr} + 2G_{14}F_{R\alpha} \\
 (GF)_{12} &= \sqrt{2} G_{11}F_{Rr} + \sqrt{2} G_{12}F_r + \sqrt{2} G_{14}F_\alpha \\
 (GF)_{13} &= \sqrt{2} G_{11}F_{R\alpha} + \sqrt{2} G_{12}F_{r\alpha} + 2G_{14}F_\alpha \\
 (GF)_{22} &= 2G_{12}F_{Rr} + G_{22}F_r + 2G_{24}F_{r\alpha} \\
 (GF)_{23} &= 2G_{12}F_{R\alpha} + G_{22}F_{r\alpha} + 2G_{24}F_\alpha \\
 (GF)_{33} &= 2G_{14}F_{R\alpha} + 2G_{24}F_{r\alpha} + (G_{44} + G_{45})F_\alpha
 \end{aligned}$$

Next the expressions for the GF matrix will be written in a way to show only their dependence upon F_R , F_{Rr} , and $F_{R\alpha}$.

$$\begin{aligned}
 (37) \quad (GF)_{11} &= G_{11}F_R + 2G_{12}F_{Rr} + 2G_{14}F_{R\alpha} \\
 (GF)_{12} &= \sqrt{2} G_{11}F_{Rr} + a \\
 (GF)_{13} &= \sqrt{2} G_{11}F_R + b \\
 (GF)_{22} &= 2G_{12}F_{Rr} + c
 \end{aligned}$$

(37 continued)

$$(GF)_{23} = 2G_{12}F_{R\alpha} + d$$

$$(GF)_{33} = 2G_{14}F_{R\alpha} + e$$

A comparison of equations (36) and (37) defines a, b, c, d, and e which are functions of $F_{R\alpha}$ at a given bond angle, α , and r_2/r_1 . Now, equation (21) may be applied and the secular determinant evaluated.

In terms of the λ 's

$$(38) \quad \lambda^3 - A\lambda^2 + B\lambda - C = 0$$

where

$$(39) \quad A = \lambda_1 + \lambda_2 + \lambda_3$$

$$(40) \quad B = \lambda_1\lambda_2 + \lambda_1\lambda_3 + \lambda_2\lambda_3$$

$$(41) \quad C = \lambda_1\lambda_2\lambda_3$$

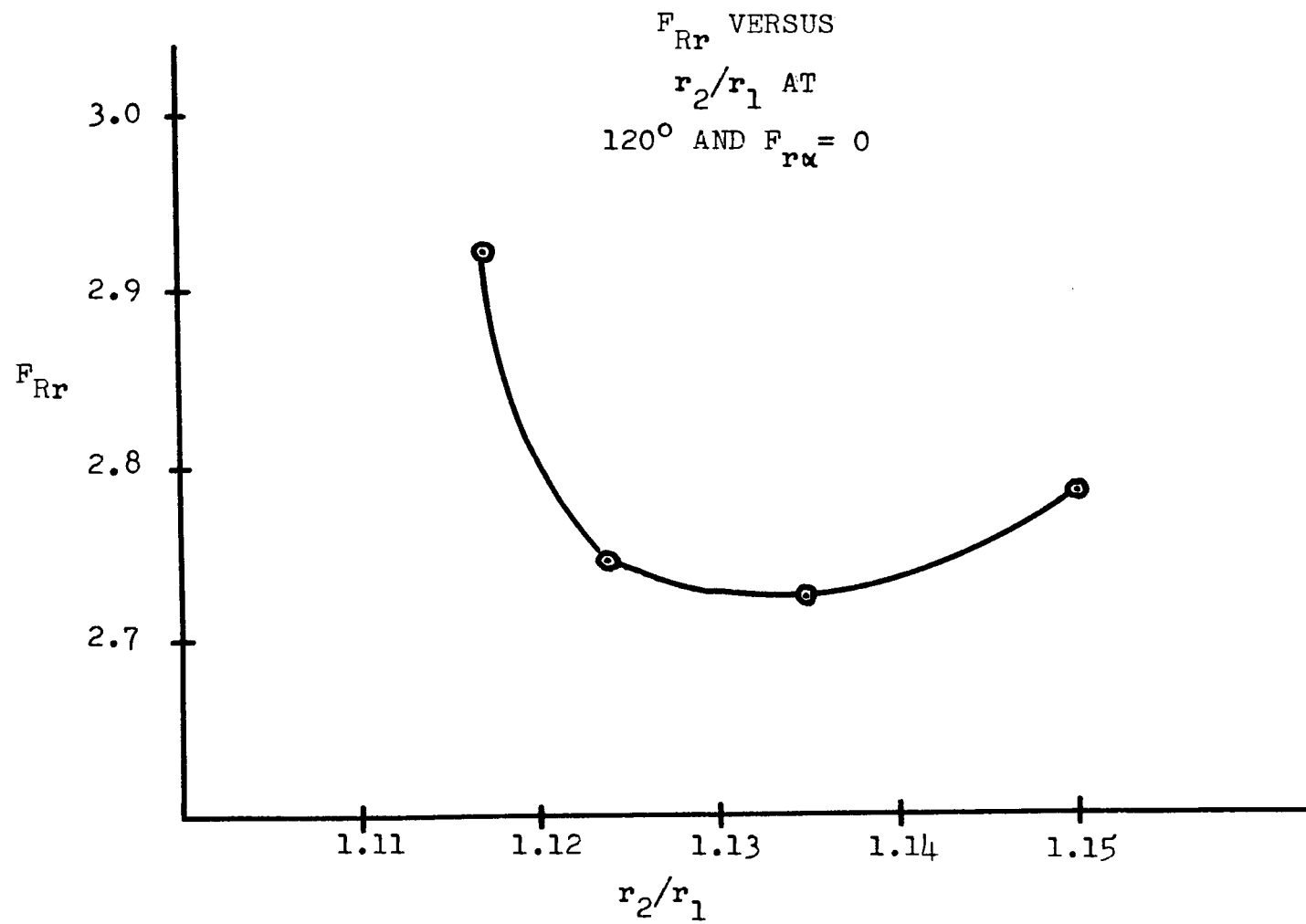
The next step is to express the values of A, B, and C in terms of F_R , F_{Rr} , $F_{R\alpha}$, a, b, c, d, and e. Thus,

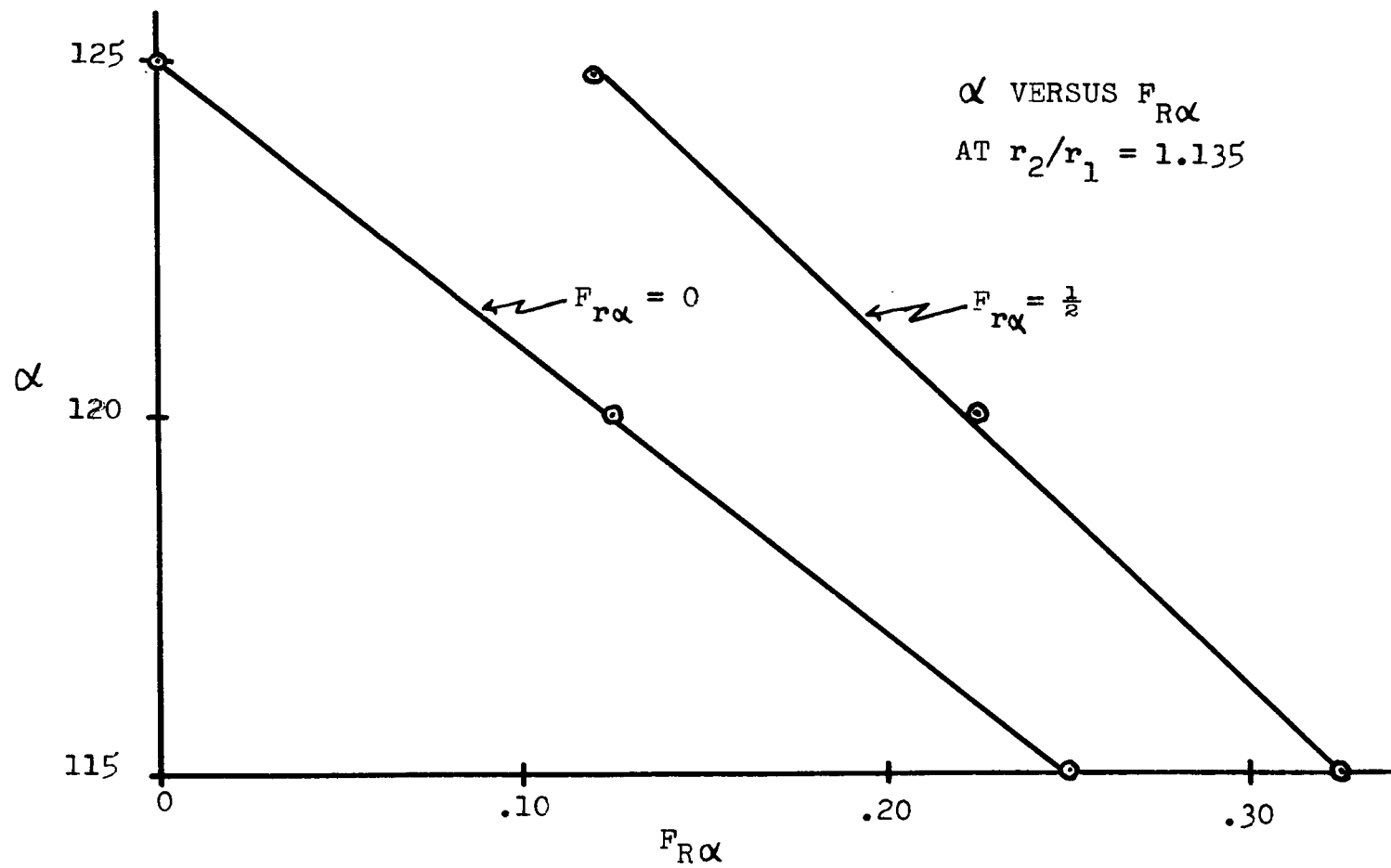
$$(42) \quad A = G_{11}F_R + 4G_{12}F_{Rr} + 4G_{14}F_{R\alpha} + e$$

$$(43) \quad B = 2G_{11}G_{14}F_RF_{R\alpha} + 12G_{12}G_{14}F_{Rr}F_{R\alpha} \\ + (4G_{14}^2 - 2G_{11}^2 - 4G_{12}^2)F_{R\alpha}^2 + (e+c)G_{11}F_R \\ + [(4e+2c)G_{12} - 2\sqrt{2}aG_{11}]F_{Rr} + [(2e+4c)G_{14} \\ - 2\sqrt{2}bG_{11} - 4dG_{12}]F_{R\alpha} + [4G_{12}^2 - 2G_{11}^2]F_{Rr}^2 \\ + 2G_{11}G_{12}F_RF_{Rr} + ec - a^2 - b^2 - d^2$$

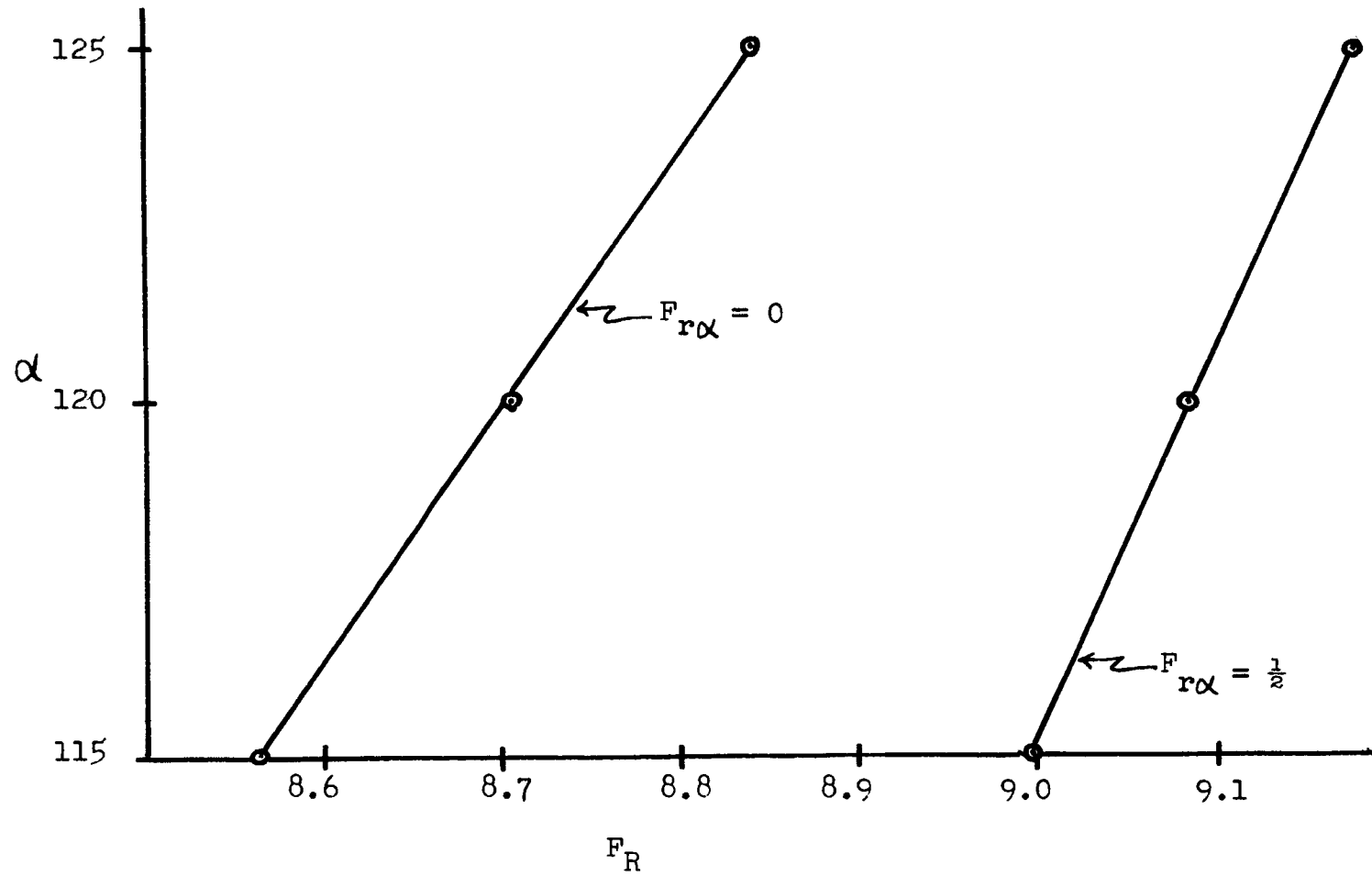
$$\begin{aligned}
(44) \quad C = & [8G_{12}^2 G_{14} - 4G_{11}^2 G_{14}] F_{Rr}^2 F_{R\alpha} + [4G_{11} G_{14} G_{12}] F_R F_{Rr} F_{R\alpha} \\
& + [8G_{12} G_{14}^2 - 4G_{11}^2 G_{12}] F_{Rr} F_{R\alpha}^2 + [2cG_{11} G_{14} \\
& - 4dG_{11} G_{12}] F_R F_{R\alpha} + [4cG_{12} G_{14} + 4dG_{11}^2 - 8dG_{12}^2 \\
& - 4\sqrt{2} aG_{11} G_{14} + 4eG_{12} G_{14}] F_{Rr} F_{R\alpha} \\
& + [4cG_{14}^2 + 4\sqrt{2} aG_{11} G_{12} - 8dG_{12} G_{14} - 2cG_{11}^2] F_{R\alpha}^2 \\
& + [4abG_{12} + 2\sqrt{2} adG_{11} - 2d^2 G_{14} - 2\sqrt{2} bcG_{11} \\
& - 2a^2 G_{14} + 2ceG_{14}] F_{R\alpha} + [2\sqrt{2} bdG_{11} - 2d^2 G_{12} \\
& - 2b^2 G_{12} - 2\sqrt{2} aeG_{11} + 2ceG_{12}] F_{Rr} + [-4G_{11}^3] F_R F_{R\alpha}^2 \\
& + [-8G_{11}^2 G_{14}] F_{R\alpha}^3 + [-d^2 G_{11} + ceG_{11}] F_R + [-2eG_{11}^2 \\
& + 4eG_{12}^2] F_{Rr}^2 + [2eG_{12} G_{11}] F_R F_{Rr} + 2abd - cb^2 - ea^2
\end{aligned}$$

It is quite apparent at this point that complications would arise if one were to try to solve for F_R , F_{Rr} , and $F_{R\alpha}$ analytically from equations (42), (43), and (44). But the complexity may be reduced to that of only solving quadratic equations. The procedure undertaken may be described as follows: F_R and F_{Rr} were determined from (42) and (43) at several values of $F_{R\alpha}$ (set I) and also from (42) and (44) at several values of $F_{R\alpha}$ (set II). Hence, if the values of F_{Rr} versus $F_{R\alpha}$ from set I are plotted on the same graph paper as those from set II,

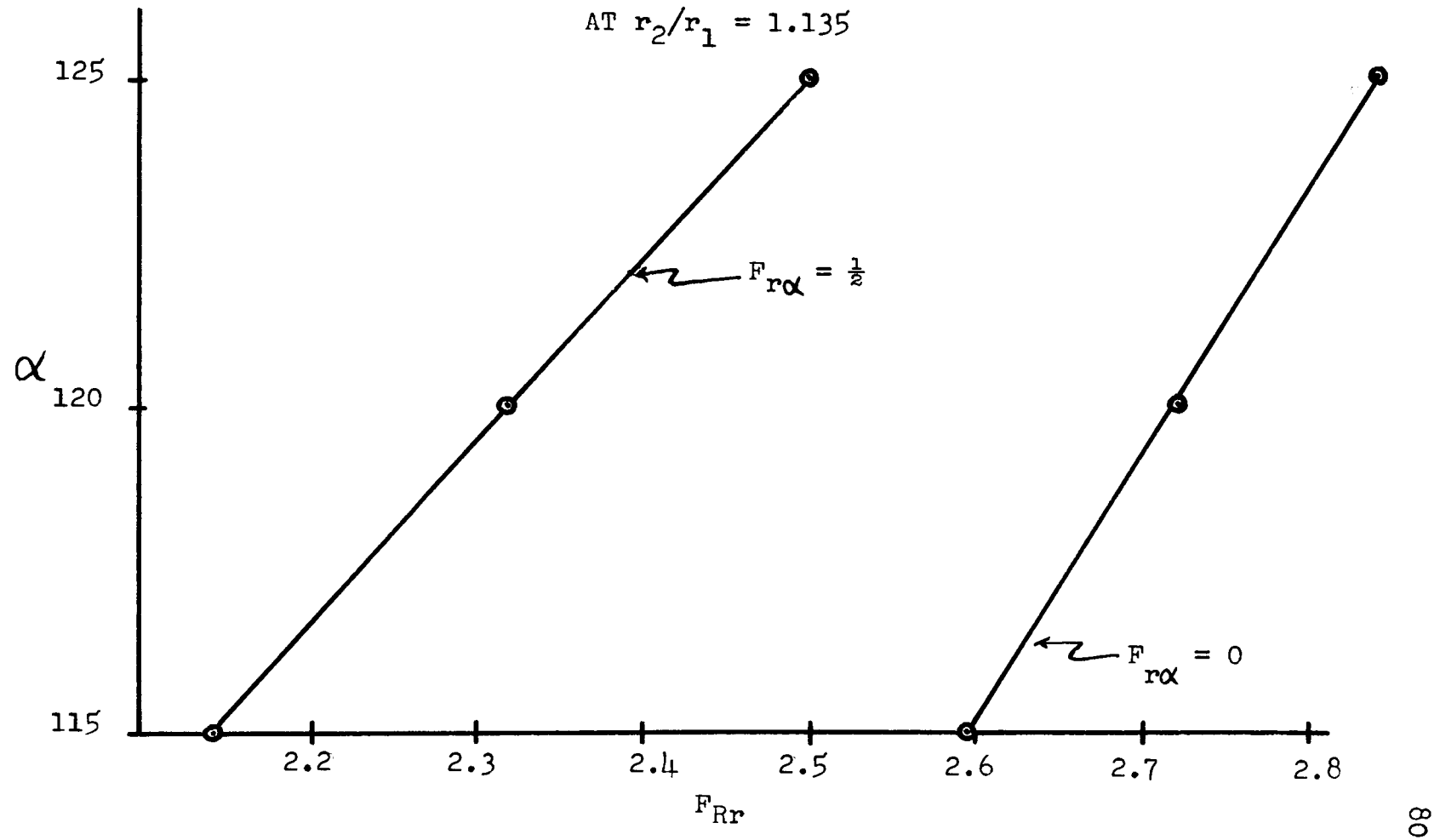




α VERSUS F_R
 AT $r_2/r_1 = 1.135$



α VERSUS F_{Rr}
AT $r_2/r_1 = 1.135$



the intersection of these two curves gives a set of force constants consistent with the observed fundamental vibrational frequencies and the assumed values of α , r_2/r_1 , and $F_{r\alpha}$.

First, consider $\alpha = 120^\circ$ and $F_{r\alpha} = 0$ and then vary r_2/r_1 . The results are summarized in the graph on page 77. F_{Rr} appears quite high in comparison with other similar interaction constants. Because of this, the remaining calculations were carried out at $r_2/r_1 = 1.135$ where F_{Rr} appears to experience a minimum.

Thus, with r_2/r_1 fixed only α and $F_{r\alpha}$ remain as variable parameters. The next task is to determine $F_{R\alpha}$, F_R and F_{Rr} at various values of α and $F_{r\alpha}$. These results are shown in the graphs on pages 78, 79, and 80. Negative values of $F_{r\alpha}$ were not included in the graphs. The values of F_R and F_α depend only upon the magnitude of $F_{r\alpha}$, hence it may seem logical in this treatment to consider negative values of $F_{r\alpha}$. However, as hinted by the graph of α versus F_{Rr} , F_{Rr} becomes larger as $F_{r\alpha}$ decreases. For $\alpha = 120^\circ$, $r_2/r_1 = 1.135$, and $F_{r\alpha} = -0.50$, F_{Rr} becomes 2.93. Because of this only positive values of $F_{r\alpha}$ were considered. Several interesting facts may be extracted from the curves shown.

First, $F_{R\alpha}$ decreases as α increases, whereas, both F_R and F_{Rr} increase as α increases. Still retaining the theme that F_{Rr} should be as small as possible this would

indicate that the angle should be less than 120° . But $F_{R\alpha}$ must also be kept small. With this reasoning, α probably should not be too much less than 120° . Second, $F_{R\alpha}$ and F_R increase as $F_{r\alpha}$ increases, whereas F_{Rr} decreases as $F_{r\alpha}$ increases. Since at the angles involved $F_{R\alpha}$ remains less than $F_{r\alpha}$ at $F_{r\alpha} = .50$, the increase in $F_{R\alpha}$ with $F_{r\alpha}$ will not be considered significant. But since F_R for a pure double N-N bond is around 13×10^5 dynes/cm, it is desirable to keep F_R relatively large. This indicates the larger values of α and $F_{r\alpha}$. The smaller values of $F_{R\alpha}$ indicate the smaller values of α and larger values of $F_{r\alpha}$. Thus, for the sake of comparison of the values of force constants obtained here with those of other molecules and ions, $F_{r\alpha}$ will be assumed to be .50 and α will be assumed to be 115° . Thus,

$\alpha = 115^\circ$	$F_R = 9.00$
$r_2/r_1 = 1.135$	$F_{Rr} = 2.14$
$F_{r\alpha} = .50$	$F_r = 4.50$
$F_{R\alpha} = .325$	$F_\alpha = 1.29$

PARCHMENT DEED

SOUTHWORTH CO. U.S.A.

100% COTTON FIBRE

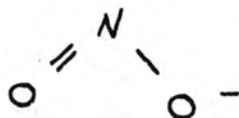
CHAPTER VII

A COMPARISON OF THE FORCE CONSTANTS CALCULATED
FOR THE HYPONITRITE ION WITH THE
FORCE CONSTANTS OF SIMILAR SYSTEMS

At first glance the values of F_α and F_{Rr} seem rather large. However, both NO_2^- (14, p. 444-446) and NO_2 (21, p. 1248-1251) have large bending force constants and large interaction constants. In the following table N_2O (18, p. 174) has been added for comparison.

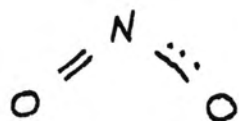
<u>Molecule</u>	F_R	F_r	F_α	F_{Rr}	F_{rr}	α
NO_2^-		7.5	1.8		1.5	132
NO_2		10.4	1.10		2.0	134
N_2O	14.6	13.7	0.49			180
N_2O_2	9.00	4.50	1.29	2.14		115

These values appear to be of similar magnitude. But we still have not discussed the similarity in the bonds involved. Let the structures be represented as follows:



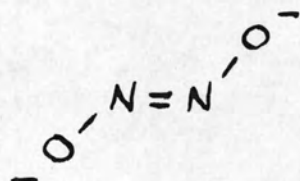
$$\alpha = 132^\circ$$

$$r_{\text{NO}} = 1.13 \text{ \AA}$$



$$\alpha = 134^\circ$$

$$r_{\text{NO}} = 1.19 \text{ \AA}$$

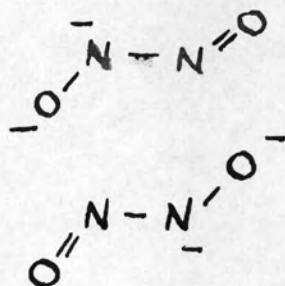


$$\alpha = 115^\circ$$

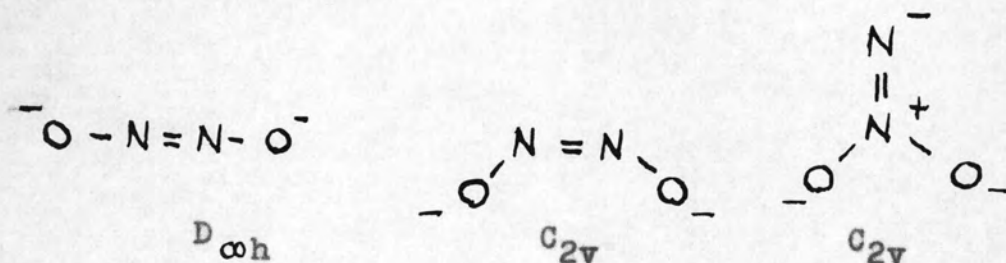
$$r_{\text{NO}} \approx 1.36 \text{ \AA}$$

$$r_{\text{NN}} \approx 1.20 \text{ \AA}$$

Resonance may be suggested to be present in the hypodinitrite ion by writing the structures



Thus, in each case the bending motion is in connection with bonds involved in resonance of what may be written as a double and a single bond about a central nitrogen atom. Millen et al. (13, p. 687-689) have treated the case of the hyponitrite ion in terms of normal coordinate theory for the C_{2h} symmetry. They also give reasons why such structures as



should not account for the observed spectra of the hypodinitrite ion. In their treatment, however, they neglected the interaction constants $F_{r\alpha}$, $F_{R\alpha}$, and F_{Rr} . In this

way they obtained the following force constants:

F_r	F_α	F_R
4.6	0.6	6.9

F_α , of course, was small in their calculation because they used ν_5 as about 370 cm^{-1} , an unobserved frequency. They used a value of 504 cm^{-1} for ν_6 , the out-of-plane distortion. This value corresponds to the value of 492 cm^{-1} used in my calculations for ν_5 , the antisymmetric in plane bending frequency. It was shown here, however, that a high bending force constant is reasonable for the assumed structure and that $\nu_5 = 492 \text{ cm}^{-1}$ is a very likely assignment. The assignment of ν_6 as 630 cm^{-1} does not involve the Raman frequencies and hence will not be discussed in detail. This assignment leads to a force constant of 1.7 md/\AA^0 . This value being rather high tends to make one feel that perhaps a fundamental lower than 400 cm^{-1} does indeed exist. If 630 cm^{-1} is not a fundamental then it should be accountable as a combination of two fundamental frequencies. Since this frequency is infrared active, it should be the sum of a g and a u species. If 492 cm^{-1} represents the u species, then this would require that a Raman active line lies at about 138 cm^{-1} . This last statement is in contradiction to the proposed hyponitrite ion structure and the observed Raman frequencies.

CHAPTER VIII

CONCLUSION

The new frequency for the hyponitrite ion at 692 cm^{-1} , although weak in the Raman effect, appears to be quite consistent with the other observed frequencies in relation to the calculated force constants. More accurate values for the force constants, bond distances, and the bond angle may be obtained if more information, such as the isotopically substituted hyponitrite spectra, were available. But the data available does point to the fact that the symmetry of the ion belongs to the C_{2h} point group. At least no contradictions are present to discredit this theory.

PARCHMENT DEED

SOUTHWORTH CO. U.S.A.

BIBLIOGRAPHY

1. Amble, Eilif and B. P. Dailey. The structure and dipole moment of hydrazoic acid. *Journal of Chemical Physics* 18: 1422. 1950.
2. Coles, D. K., E. S. Elyash, and J. G. Gorman. Microwave absorption spectra of N_2O . *Physical Review*, ser. 2, 72:973. 1947.
3. Coles, D. K. and R. H. Hughes. Microwave spectra of nitrous oxide. *Physical Review*, ser. 2, 76:178. 1949.
4. Crawford, B. L. and W. J. Horwitz. A Raman apparatus for quantitative polarization measurements. *Journal of Chemical Physics* 15: 268-274. 1947.
5. Edsall, J. T. and E. B. Wilson, Jr. Polarization of Raman lines. *Journal of Chemical Physics* 6: 124-127. 1938.
6. Gould, Edwin S. *Inorganic reactions and structure*. New York, Henry Hold, 1955. 470 p.
7. Haunschild, Willard Marion. The vibrational spectrum and rotational isomerism in tetrachloroethane. Ph.D. thesis. Berkeley, University of California, 1954. 43 numb. leaves. (Microfilm)
8. Herzberg, Gerhard. *Infrared and Raman spectra of polyatomic molecules*. New York, D. Van Nostrand, 1945. 632 p.
9. Kuhn, L. P. and E. R. Lippincott. Vibrational spectrum and structure of the hyponitrite ion. *Journal of the American Chemical Society* 78: 1820-1821. 1956.
10. LeFevre, R. J. W., W. T. Oh, I. H. Reece, and R. L. Werner. Infra-red absorption spectra of metal hyponitrites. *Australian Journal of Chemistry* 10: 361-364. 1957
11. Magnuson, Dale W. Determination of the two-dipole moment components in nitrosyl fluoride. *Journal of Chemical Physics* 19: 1071. 1951.
12. Millen, D. J., C. Polydoropoulos, and D. Watson. Dissociation in solid solution in potassium bromide. The monomeric hyponitrite ion NO^- . *Proceedings of the Chemical Society*. 1957: 18.

13. Millen, D. J., C. Polydoropoulos, and D. Watson. Normal co-ordinate analysis for trans-centro-symmetric X_2Y_2 molecules: application to the hyponitrite ion. *Journal of the Chemical Society* 1960: 687-691.
14. Newman, Roger. Polarized infrared spectrum of sodium nitrite. *Journal of Chemical Physics* 20: 444-446. 1952.
15. Nielson, J. R. The filling of a spectrograph with light considered as a geometrical radiation problem. *Journal of the Optical Society of America* 20: 701-718. 1930 .
16. Nielson, J. R. Theory of condensing lenses for Raman tubes of small volume. *Journal of the Optical Society of America* 37: 494-499. 1947.
17. Partington, J. R. and C. C. Shah. Investigation of hyponitrites. *Journal of the Chemical Society* 1931, p. 2071-2080.
18. Pauling, Linus. The nature of the chemical bond. 3d ed. New York, Cornell University, 1960. 644 p.
19. Rank, D. H. and R. E. Kagarise. Empirical convergence correction of depolarization measurements. *Journal of the Optical Society of America* 40: 89-92. 1950.
20. Stamm, Robert F. A fast grating spectrograph, accessories and techniques for studying the Raman effect. *Industrial and Engineering Chemistry, Analytical Edition* 17: 318-331. 1945.
21. Weston, Ralph E. Jr. Infrared spectrum of $N^{15}O_2$ and force constants of NO_2 . *Journal of Chemical Physics* 26: 1248-1251. 1957 .
22. Wilson, E. Bright, Jr., J. C. Decius, and Paul C. Cross. *Molecular vibrations*. New York, McGraw-Hill, 1955. 388 p.
23. Yost, Don M. and Horace Russell. *Systematic inorganic chemistry*. New York, Prentice Hall, 1944. 423 p.